École polytechnique de Louvain

Analysis and correction of the hysteresis effect in a gas micro-sensors

Author: **Maugan BELLEFLAMME**
Supervisors: **Prof. Flavio ABREU ARAUJO, Dr. Yann DANLÉE**
Readers: **Prof. Laurent FRANCIS, Dr. Nicolas JULÉMONT**
Academic year 2023–2024
Master [120] in Electro-mechanical Engineering

Acknowledgement

Firstly, I would like to thank Prof. Flavio Abreu Araujo and Dr. Yann Danlée for offering me this thesis topic. The analysis and understanding of complex systems in the field of signals and systems is very exciting. I would like to thank them for being available to answer my questions, and for their follow-up, advice and feedback throughout the year, all of which aimed to improve the quality and accuracy of this work.

I would also like to thank the company VOCSens for allowing me to do this thesis, based on its experiments data and technology.

I would like to thank the Prof. Laurent Francis and the Dr. Nicolas Julémont for agreeing to be part of my jury. Anatole Maureaux was always available for answering my questions throughout the year. I thank him for this continuous support.

Finally, I would like to thank my parents and family for their support throughout my studies and this year in particular, as well as my friends for making me appreciate these years of study and my flatmates for the time spent together on the Kotangente project.

Abstract

The objective of this thesis is to analyse and correct the effect of hysteresis in micro-sensors. Hysteresis is a non-linear phenomenon commonly observed in various physical systems. This hysteresis poses significant challenges for signal modelling and system control. This thesis focuses on the identification, modelling and mitigation of the hysteresis effect in a gas micro-sensor. The standard score is used for normalisation. For filtering, we use wavelets with a filtering threshold and a Savitzky-Golay filter. For curve modelling, sigmoids are used and for hysteresis simulation a Taylor expansion is used. The model achieves good result. It cancel the hysteresis effect on the trained data, with an MSE of 0.074.

Contents

Introduction

Hysteresis is a phenomenon discovered in 1890 by the physicist Sir Alfred Edwing. This phenomenon was initially studied in the context of magnetic hysteresis, but also manifests itself in many other areas of physics such as the plasticity of materials, friction, ferroelectricity and superconductivity. It was then developed in various fields such as biology and economics.

Hysteresis represents the mismatch between the input excitation and the resulting output, causing a non-linear, non-bijective and often complex relationship between the two. This non-linearity complicates the modelling and prediction of system behaviour, particularly in microsensors where accuracy is paramount.

Various methods have been developed in the last century and this one to model the hysteresis effect. This is becoming increasingly well known and understood for common hysteresis effects such as magnetic hysteresis or the hysteretic behaviour of piezoelectrics. For the less analyze hysteresis effects, these are poorly modelled and there is still much unknown about them.

This master's thesis focuses on the analysis and correction of the hysteresis effect in gas microsensors. The main objective is to develop robust methods for identifying, modelling and mitigating this effect in order to improve the accuracy of microsensors.

Chapter 1

State of Art

1.1 Hysteresis effect

The aim of this master's thesis is to analyse and to model the effect of hysteresis in a micro-sensor. The hysteresis effect appears in various physical phenomena,mainly in the electrical and mechanical fields. The best known of these phenomena is the magnetisation of ferromagnetic materials [4][5][22] but it is also found in other ones like the plasticity of materials [24], the piezoelectric [6] and the superconductivity [2][9]. The hysteresis effect can be identified in a system which takes as input an excitation signal (magnetic field, force, etc.) and returns as output the input signal altered by the hysteresis effect. This effect causes non-linear relationship between output and input, making its modelling complicated to realize.

The hysteresis effect in a system is defined by two characteristics, the memory and the branching [5]. The memory is the capacity of the system to remember past states of itself and to be influenced by them. The branching describes the ability of the system to react differently when the input signal decreases or increases. In other words, depending on the previous state of the system and the sign of the derived input signal, the output value will take on different values. For example, in the case of a ferromagnetic element, the flux density (B) does not vary linearly in relation to the magnetic field (H) and varies differently when the magnetic field increases or decreases, as shown in the figure 1.1.

This curve shown in the figure 1.1 is also known as the hysteresis loop or cycle. This is because we are no longer dealing with a transfer function where, for a certain value of the field H, we have a unique value of the flux density B. Here we have several values of flux B possible for a single value of field H. These different values depend on the memorization and the branching characteristics of the hysteresis effect.

We will describe this hysteresis effect step by step on this example. Initially, before the magnetic field (H) is applied, the ferromagnetic material has no induced magnetic flux (B). This starting point is represented by the point 0 in figure 1.1. When the field H is increased, the element becomes charged (magnetised). This charge is represented by the dotted line in blue, the curve between 0 and a. At a certain value of applied magnetic field, the material reaches magnetic saturation and the magnetic flux can no longer circulate and saturates (point a). If the magnetic field (H) is reduced after saturation is reached, the magnetic flux (B) also decreases, but it follows a different path than that of the field increase. It follows the upper path of the curve from a to b. When the magnetic field (H) returns to zero, the magnetic flux (point b) is not zero as it was initially (point O). There is now a certain level of residual magnetic flux, represented by the offset in the curve. This means that even when the magnetic field is null, the material retains some residual magnetisation. Inversely, when the magnetic field increases starting from the minimum value at point d, a residual magnetic flux is also detected on point e. The light blue area represents thus all the possible values of the magnetic flux in relation to the increase and decrease of the magnetic field.

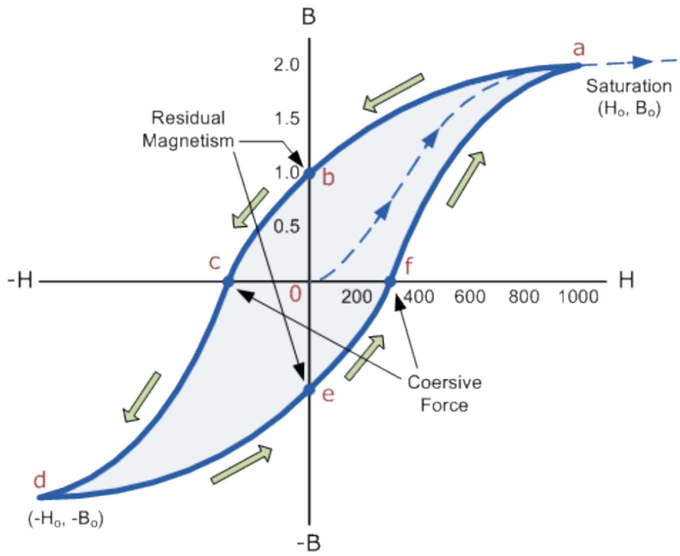

Figure 1.1: Diagram showing the magnetic hysteresis loop within a ferromagnetic core. Image borrow from the publication "Electronics Tutorials - Magnetic Hysteresis" [4]

1.2 Modelisation of hysteresis

Hysteresis is a fairly well-known phenomenon by now and several types of model exist for the different types of hysteresis. The majority of these models have been designed for the effect of hysteresis due to the magnetisation of ferromagnetic materials, the electrical charge of piezoelectric actuators or the strain energy density in materials.

Modelling the effects of hysteresis is important, as it allows us to better understand the physical phenomena, to predict their behaviour and consequently to better control the media where this effect is present [6][8][9].

Modelling hysteresis is not a straightforward task. The hysteresis effect is a non-linear phenomenon that cannot be represented by a function. For this reason, there are various models, each with different qualities depending on their use. We will look at the different approaches and characteristics of these models.

1.2.1 Rate-Dependent and Rate-Independent hysteresis model

A first way of differentiating models is according to the response of the model to the input. There are two types:

Rate-independent The most basic models depend only on the magnitude of the input and not its frequency. These models are called rate-independent and are often used for low-frequency models. They are expressed as follows:

$$\frac{dy(t)}{dt} = g\left(x, y, \text{sign}\left(\frac{dx}{dt}\right)\right)\frac{dx}{dt} \tag{1.1}$$

Here the hysteresis model $g(...)$ depends only on the magnitude of x and not on its derivative. The most usual models are the Preisach model, the Prandtl-Ishlinskii model and the Maxwell model.

Rate-dependent : Rate-dependent models take into account the frequency of the input signal when parameterising the system. The shape of the hysteresis curves therefore depends on the time derivative of the input. These models take the following mathematical form:

$$\frac{dy(t)}{dt} = g\left(\frac{dx}{dt}, y, \operatorname{sign}\left(\frac{dx}{dt}\right)\right)\frac{dx}{dt} \tag{1.2}$$

This type of model is more complex than the Rate-Independent models. You need a lot of data in the different frequencies to capture the full hysteresis behaviour. However, this type of model is increasingly being studied and used because it is much more accurate for high-frequency applications and is closer to reality.[3].

1.2.2 Phenomenological and Physical Models

There is also another way of differentiating hysteresis models into two categories either by the physics behind the curve or by the behaviour of the hysteresis. In the case of a physical model, this is based on the equations that attempts to describe the physics behind the phenomenon. Whereas a phenomenological model simply tries to fit a curve onto the experimental values of the hysteresis without really explaining it. Figure 1.2 categorizes the different existing models following the criteria described here above.

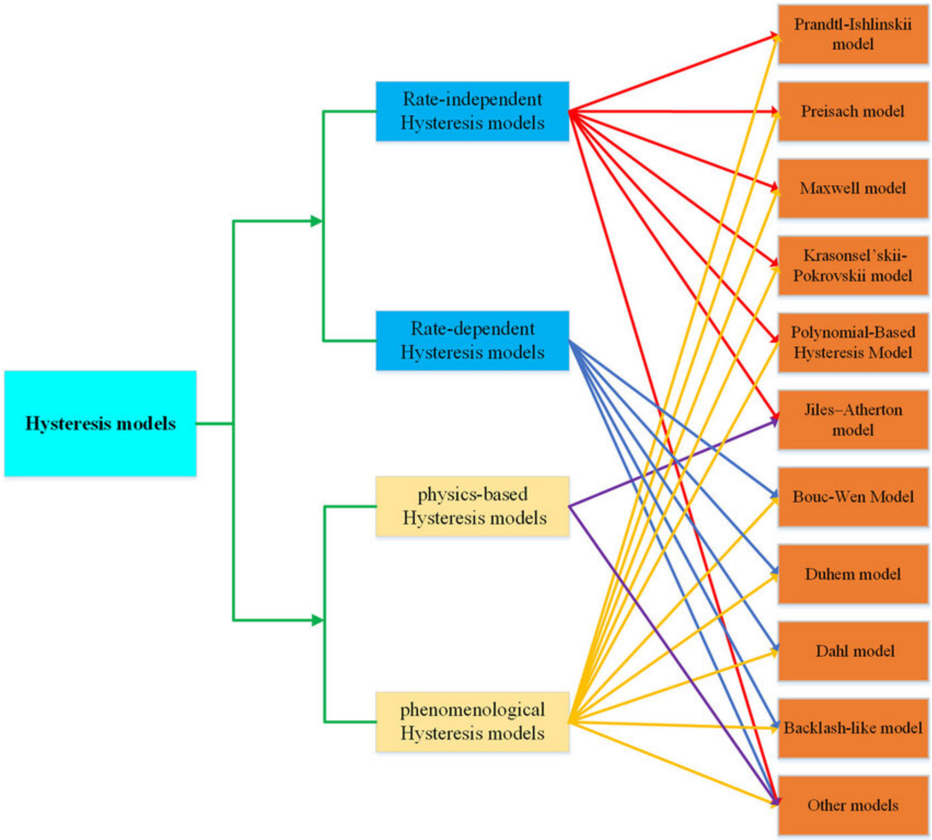

Figure 1.2: Chart of different existing hysteresis models, image borrowed from the paper [6]

1.2.3 Asymmetry, Pinching and Inversible

The four other main characteristics of the models are asymmetry, pinching, degradation and inversibility. They will be described briefly:

Asymmetry : Most basic models focus on hysteresis that is symmetrical with respect to the origin (as in magnetisation phenomenon) or with respect to the $y = x$ line (as in elasticity phenomenon). An asymmetric hysteresis can be seen in figure 1.3. For the rest of the hysteresis curves, most are not symmetrical, such as piezoceramic [8].

Pinching : Pinching is the flattening or crushing of the hysteresis curve, usually in its most linear part (as shown in figure 1.4). This gives an hysteresis curve more of a "lobe" shape than an S shape. This type of hysteresis is often found in memristors [28].

Degradation The degradation effect in hysteresis refers to a drift in the hysteresis curve caused by cycling or reaching saturation. This drift can create either a linear shift or a rotational change in the hysteresis loop [3].

Inversibility : The inversibility of a model is essential to compensate the hysteresis effect and control such a system[6][8][9][11]. Models are mathematical expressions which are not all invertible or very difficult to invert.

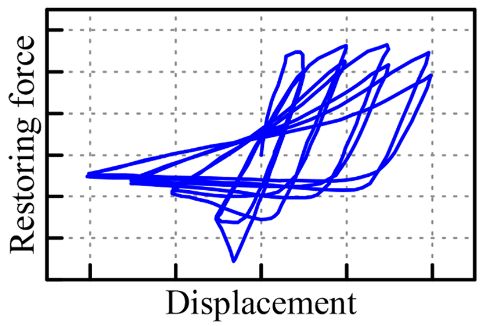

Figure 1.3: Asymmetrical characteristic of hysteresis

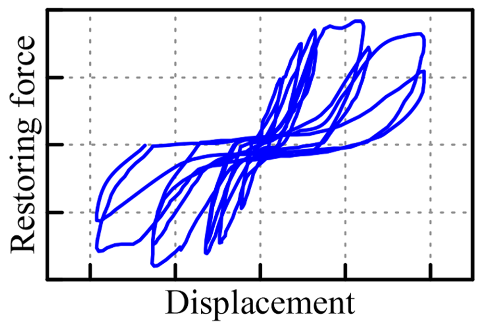

Figure 1.4: Pinching characteristic of hysteresis

Figure 1.5: Characteristics of hysteresis, image borrowed from the paper [3]

1.2.4 Data-driven and model-driven

There are two approaches to the hysteresis effect, either a model approach or a data approach [3]. The model-driven approach consists of choosing a model based on the shape of the experimental data and then identifying the model parameters using these data. For this approach, the choice of model is crucial and must have the key hysteresis factors.

In the data-driven approach, a mathematically universal model is trained using a convergence method [26]. Data is a much more important factor for this type of model.

With the emergence of machine learning and deep learning algorithms, the data-driven approach has become more interesting. Indeed, using neural network techniques [7] or support vector machine techniques [27], it has been shown that it is possible to simulate correctly an hysteresis.

1.3 Hysteresis model

There is a large number of hysteresis models. We will briefly review the most commonly used without aiming to build an exhaustive list.

1.3.1 Prandtl-Ishlinskii

The Prandtl-Ishlinskii model is one of the most widely used models for simulating magnetic hysteresis. The great advantage of this model is its invertibility [17]. In fact, this model assembles several linear mathematical expressions into a non-linear function. These expressions are called [9] operators and there are two of them:

- the play operator :

$$\mathcal{F}_{r_i}[x(t)] = \max\left(\min\left(x(t) + r_i, \mathcal{F}_{r_i}[x(t_{k-1})]\right), x(t) - r_i\right) \tag{1.3}$$

  with the initial condition :

$$\mathcal{F}_{r_i}[x(0)] = \max\left(\min\left(x(0) + r_i, M_0\right), x(0) - r_i\right) \tag{1.4}$$

  Where

  $x(t)$ is the input signal

  r_i is the operator threshold

  t_k the time step

  M_0 the initial condition

- the stop operator :

$$\mathcal{F}_{r_i}[x(t)] = \min\left(r_i, \max\left(-r_i, x(t) - x(0) + \mathcal{F}_{r_i}[x(t_{k-1})]\right)\right) \tag{1.5}$$

  with its initial condition :

$$\mathcal{F}_{r_i}[x(0)] = \min\left(r_i, \max\left(-r_i, M_0\right)\right) \tag{1.6}$$

These two operators are assembled by each other by weighted addition:

$$y(t) = \sum_{i=1}^{n} p_i \mathcal{F}_{r_i}[x(t)] \tag{1.7}$$

where p_i is the weight for the operator with a threshold r_i.

By stacking different operators with different thresholds r_i and weights p_i, this model is able to recreate the non-linear behaviour of hysteresis. This function is easily invertible, making it very interesting for the purpose of compensating for a system subject to hysteresis. The basic model is symmetrical, although asymmetrical variants exist. Similarly, the basic model is rate-independent but rate-independent variants exist [18][19].

1.3.2 Duhem model

Duhem's model is widely used for modelling hysteresis with little known physical phenomena ('black box')[22]. The great advantage of this model is that it has a clear mathematical expression and that an appropriate adjustment of the model parameters can accurately reflect the various non-linearity of the hysteresis [20]. Its general form is expressed as follows :

$$y(t) = f(x(t), u(t))g(\dot{u}(t)) \tag{1.8}$$

where:

$y(t)$ is the output,

$x(t)$ is the state vector variable,

$u(t)$ is the input signal,

f and g are functions that describe the system's behavior.

This model is fairly general. Everything depends on the form of f and the parameters we give it. For asymmetry, all you need is an asymmetric f function. For rate-dependence, all you need is $\dot{u}(t)$ in the state vector of the f function [21].

1.3.3 Artificial Intelligence (AI) and Machine learning model

There are more and more models using various AI and machine learning techniques. Most of these are added to an existing model.

The Particle swarm optimization algorithm is used to optimise a Duhem model [12].

In machine learning, a hysteresis Duhem model has also been developed in a neural system, allowing the weight of the neural network to be linked to the parameter of the Duhem model [13].

The same applies to a Prandtl-Ishlinskii model and a [14] neural network.

> In deep learning, a neural model that has been successfully applied to rate-dependent and rate-independent hysteresis is the Elman neural network (ENN).
>
> A convolution neural network (CNN) has also been tried for hysteresis modelling [16].

There are lots of different AI and machine learning techniques. They generally give a better result than classical models but require a high volume of data.

Chapter 2

Problem statement

2.1 Context and objective

This master's thesis is being carried out with VOCSens. VOCSens is a company developing a new micro-sensor technology: 'CMOSEnvi'. The aim of this technology is to measure the presence and concentration of different gases with a single micro-sensor. To measure the concentration of these different gases, VOCSens uses different chemiresistive materials such as rGO-PEI to measure CO_2, PAni:PSS-MWCNT-Fe to measure CO or PPy for ammonia. In our case, the hysteresis effect was observed on the ammonia sensor.

These chemiresistive materials give a resistance value and these are converted into concentration by this formula $\frac{R-R_0}{R_0}$. R is the resistance of the sensor and R_0 is the resistance of the sensor at 20°C and 50% relative humidity. As the values of R_0 are not available for now, the values will be expressed in terms of resistance (Ohm) and not concentration (%) throughout this master thesis.

The ammonia micro-sensor is therefore a chemiresistive gas sensor composed of a gas-sensitive conductive polypyrrole polymer (PPy). This polymer has been modified to be more sensitive to ammonia. It is deposited as a thin film, ideally less than 1 µm thick, completely covering interdigitated electrodes. The gas absorption process on this surface, although complex, can be simplified: the gas molecules form hydrogen bridges with the polymer surface.

When a target gas comes into contact with the sensitive material, it interacts with the surface, causing chemical reactions such as adsorption (where gas molecules bind to the surface) and, in some cases, redox (reduction-oxidation) reactions with ions present on the surface. These interactions modify the concentration of charge carriers (electrons or holes) in the material. For example, reducing gases (such as CO) supply electrons, thereby increasing the concentration of free electrons and reducing the resistance of the material. On the other hand, oxidising gases (such as NO_2) capture electrons, reducing the concentration of free electrons and increasing resistance. Modelling this physical phenomenon is quite complicated.

The aim of this master thesis is to study and understand this hysteresis effect. Indeed, during tests in a climatic chamber, an hysteresis effect caused by the temperature and the relative humidity of the resistance of the micro-sensor has been detected. The first step is to determine how temperature and relative humidity affect the resistance behaviour. Based on this result, we modelize the hysteresis effect and finally we look after solutions for counteracting the effect. Given that the hysteresis effect in the sensor is a new problem, the possible solutions are not yet known.

2.2 Data and Analysis

For this analysis, I was provided with data sets from two experiments carried out in a climatic chamber. In these experiments, only two parameters change, temperature and relative humidity. The composition of the air inside the climatic chamber is not modified, f.i. no other gases are added to the air. The result is the evolution of the value of the electrical resistance of the micro-sensor during each of the experiments.

In the first experiment, six temperature steps were tested, each of five Celsius degrees, between twenty-five and fifty Celsius degrees. Each step lasts for six hours. During each step, the humidity rises and falls in steps, giving the shape of an 'Aztec' pyramid, as shown in figure 2.1. The rate of change of relative humidity is around 5% per minute. The abscissa is expressed in mm-dd hours.

For the second experiment, they used the same parameters in the climate chamber as for the first. This time, the humidity did not rise and fall in steps but in a constant manner, giving a triangle shape signal. The relative humidity and temperature parameters are displayed on the graph 2.2. This time the changes in humidity are slower, of the order of 0.6 % per minute

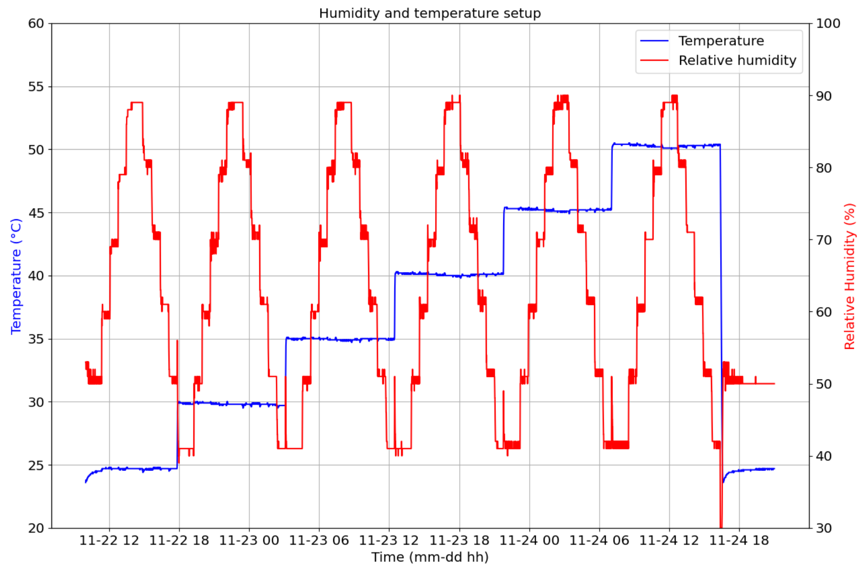

Figure 2.1: Temperature and relative humidity parameters for the first experiment inside the climatic chamber

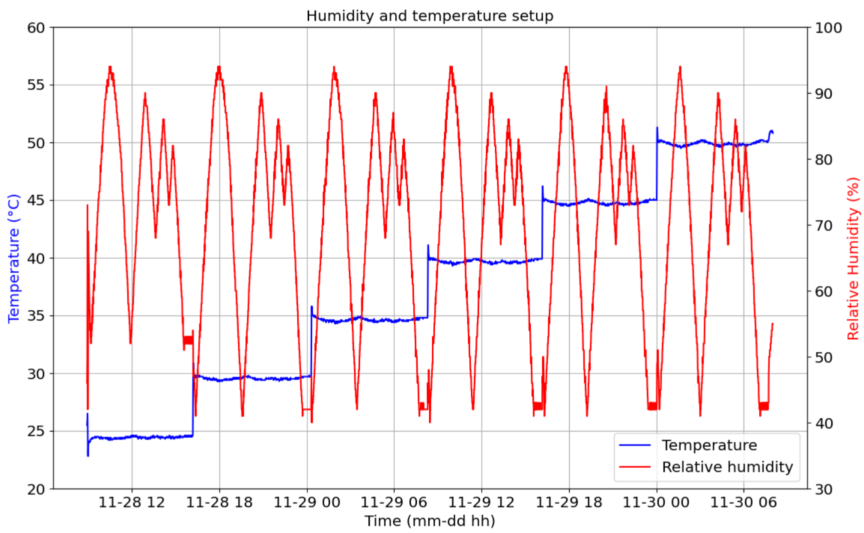

Figure 2.2: Temperature and relative humidity parameters for the second experiment inside the climatic chamber

The variation in resistance of one of the micro-sensors during the second experiment can be seen on the graph 2.3. You can see that the resistance value is influenced by temperature and relative humidity but the effect of hysteresis is not really visible.

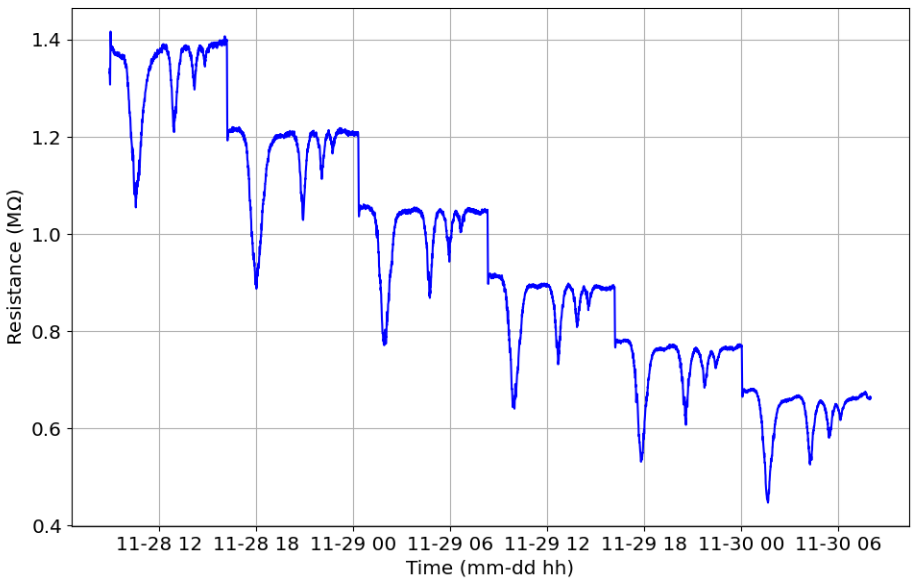

Figure 2.3: Hysteresis effect on the micro-sensor for the second test

If we now plot the resistance as a function of relative humidity and temperature, we obtain this figure 2.4

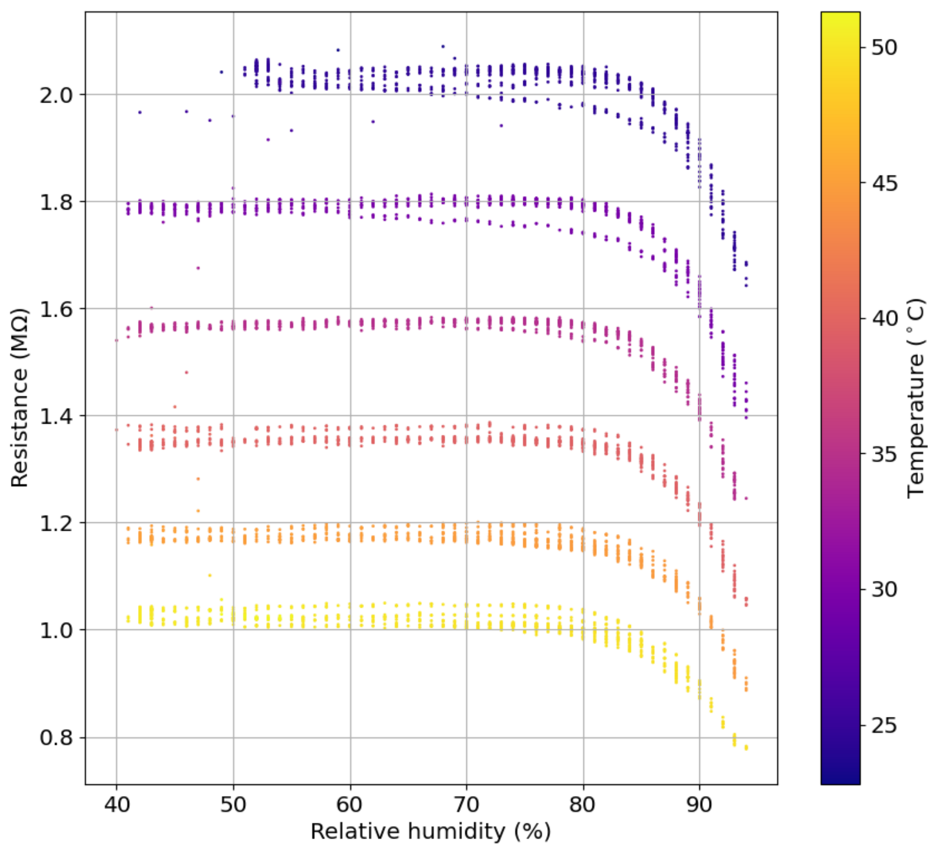

Figure 2.4: Hysteresis effect on the micro-sensor for the second test

On figure 2.4 we can see the hysteresis effect. There are several different output value paths depending on the sign of the input signal derivative. The effect is most visible on a video showing the evolution of the resistance with time. This video is available **HERE**[1]. Similar hysteresis curves are obtained for the first experiment, which can be seen in the appendix 6.2.

We start the analysis with the shape of the hysteresis and its behaviour. The first step is to define the parameters of the hysteresis system. In the experiments, for each period of 6 hours, the temperature is fixed and the relative humidity

[1]https://youtu.be/5NH7nt8qhUU

changes. The temperature will be a state parameter of the system and will not change as a function of time. Humidity will be our system input signal. We will therefore have a time-invariant system and each modelling of the system will be done at a constant temperature.

Assumption 1 *The temperature is time-invariant, leading to the following system:*

$$y(t) = f(T, y(t-1), h(t), \dot{h}(t), \mathrm{sign}(\dot{h}(t)) \tag{2.1}$$

where,

$y(t)$ *is the the resistance of the micro-sensor*

T *is the constant temperature*

$y(t-1)$ *is the previous value of the resistance*

$h(t)$ *is the relative humidity varying with time*

Next, we need to determine whether the system is influenced by the frequency of the input signal. For both experiments, the humidity changes very slowly. We assume that the frequency is low and that our system is Rate-Independent. This gives us :

Assumption 2 *The system is Rate-Indenpendant :*

$$y(t) = f((T, y(t-1), h(t), \mathrm{sign}(\dot{h}(t)) \tag{2.2}$$

For the shape of the hysteresis, we are dealing with a pinched and asymmetric hysteresis. Before 70%, the hysteresis curve is flat and thin. After 70%, the resistance decreases and plunges asymptotically. On the way back (humidity goes back down), the hysteresis takes a different, wider path, creating a lobe.

For asymmetry, it depends on how we represent our hysteresis. In the case of relative humidity, this is expressed as a percentage. It ranges from 0 to 100 %. If we now decide that, hypothetically, our hysteresis goes from -100% to 100%, we would have a ‘phantom’ part to our hysteresis in the negative domain of the x-axis. This phantom part would be the symmetrical image of the positive part. Figure 2.5 represents a schematic view of a potential symmetrical hysteresis in our case. The case of symmetry or non-symmetry is therefore ignored.

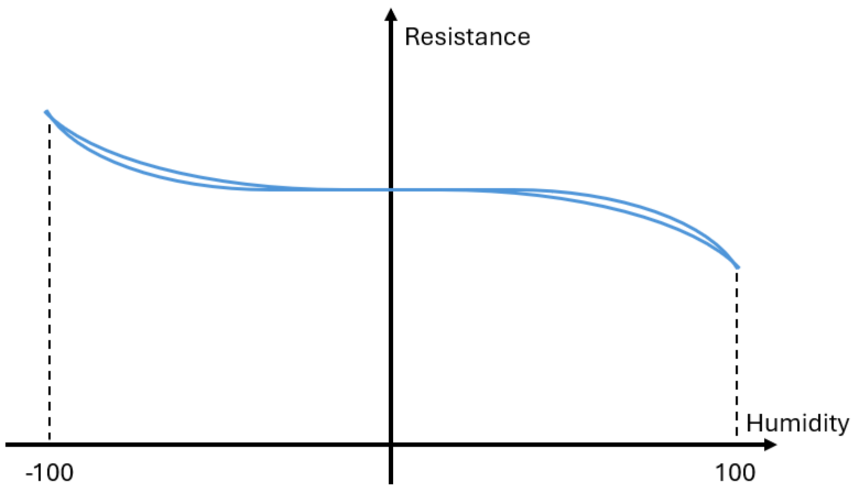

Figure 2.5: Symmetrical representation of hysteresis

When the hysteresis curve returns (the relative humidity drops again), it tends towards a resistance value that is slightly different from the starting value. This type of phenomenon can be likened to ageing or degradation. We don't know whether this phenomenon comes from the hysteresis or from another part of the micro-sensor. To facilitate initial modelling, this degradation will be neglected.

Assumption 3 *The degradation is neglected.*

We concentrate now on the influence of the parameters on the hysteresis curve. The first thing we can determine is the shift in hysteresis as a function of temperature. For a relative humidity of less than 70%, the resistance of the micro-sensor is considered constant. This constant decreases almost linearly with temperature. It is assumed that the constant depends only on temperature and not on relative humidity.

Assumption 4 *The horizontal asymptote (H_{a}) depends only on temperature and follows this relationship with temperature.*

$$y(t) = H_{\text{a}}(T) + g(T, y(t-1), h(t), \text{sign}(h(t))) \tag{2.3}$$

with,

$$H_{\text{a}}(T) = a_{\text{Ha}}T + b_{\text{Ha}} \tag{2.4}$$

and,

$$\lim_{H \to 0} y(t) = H_{\text{a}}(T) \tag{2.5}$$

Then, at relative humidity levels above 70%-75%, the resistance begins to decrease. The value at which this inflection occurs is fixed and depends on neither temperature nor relative humidity. We will call this value the decreasing point of our model (P_{inf}).

Assumption 5 *The decreasing point does not depend on relative humidity or temperature and is therefore constant.*

$$P_{\text{dec}} = \text{Constant} \tag{2.6}$$

Finally, as the humidity increases and passes a certain threshold (85%-90%), it decreases steadily. The slope of this oblique asymptote (O_a) seems to depend solely on temperature. The greater the temperature, the smaller the slope. This leads to a new hypothesis :

Assumption 6 *At around 100 relative humidity, the curve tends asymptotically (obliquely) as a function of temperature.*

$$\lim_{H \to 100} (y(t) - (a_{\text{Oa}} T + b_{\text{Oa}})) = 0 \tag{2.7}$$

2.3 Model Characterization

When relative humidity increases, the path is almost always the same. So when relative humidity falls, the path seems to depend very much on the initial relative humidity (the start of the descent). For the rest, we assume that there are two different expressions of the path, one for the upward path and one for the downward path.

Assumption 7 *The parameter value of the hysteresis system depends on the sign of the derivative*

$$g(t) = \begin{cases} g_1(...), & \text{if} \frac{dh}{dt} >= 0 \\ g_2(...), & \text{if} \frac{dh}{dt} < 0 \end{cases} \tag{2.8}$$

The aim of this thesis is therefore to cancel out this hysteresis effect. The model must not be invertible but predictive. Indeed, we have access to the value of the hysteresis thanks to the value of the resistance. We need to be able to predict the next value of hysteresis as a function of temperature, previous state and relative humidity and subtract this prediction from the value of our resistance with the objective to have a minimal error..

Assumption 8 *The absolute difference between the resistance value and its prediction should be as close as possible to zero.*

$$Err = |y(t) - \hat{y(t)}| = 0 \tag{2.9}$$

To continue further the hysteresis analysis, the data must be cleaned. In the next chapter, we'll look at filtering and slicing the data. Then, in another chapter, we will apply various methods to model the hysteresis. Finally, we will discuss the results.

Chapter 3

Data analysis and processing

In this chapter, we concentrate on the processing of the data. For good modelling, we need clean, non-intrusive data. In fact, data processing is important to improve the information in the data and to obtain better quality models. We need to remove spurious data and reduce noise in the data. As mentioned in the previous chapter, two experiments were carried out. This gives us two sets of data. The raw data can be found in the appendix 6.2.

During the experiments, eight sensors were placed in the climate chamber but only three worked correctly. These three sensors are #102, #107 and #108. On each sensor, there are eight channels of measurements. As shown on the raw data in appendix 6.2, all these channels did not work correctly and did not give valid measurements. In total, with the three selected sensors, resistance measurements from ten channels are valid.

For the analysis of the data, we concentrate on experiment 2 because it provides continuous data which makes it easier to understand and to model the hysteresis effect. Indeed, in the first experiment, as the temperature and humidity change in steps, clouds of points are obtained for a certain temperature and relative humidity. Whereas in the second experiment, the continuous change in relative humidity gives a continuous change in sensors resistance. Therefore we use experiment 2 for modelling and experiment 1 for validation of the model.

3.1 Normalization

First, we need to align the data from the various micro-sensors with each other. For each channel of each sensor, the value of the initial resistance is different, as shown in Figure 3.1.

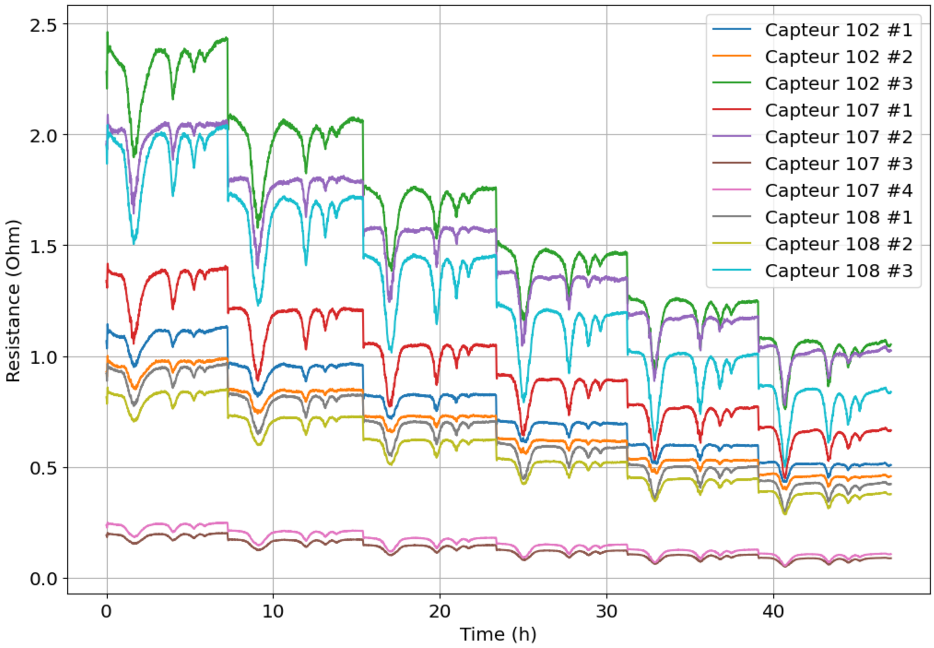

Figure 3.1: Resistance evolution for each sensor

To bring all the resistance measurements down to a consistent set of values, we'll apply a normalisation process to the data. There are various methods for performing this standardisation. We test several of them and select the best one.

3.1.1 Min-max normalization

A first normalisation technique is to use the min-max normalization [29] method. This method is expressed as follows:

$$x' = \frac{x - \min(\mathrm{x})}{\max(\mathrm{x}) - \min(\mathrm{x})} \tag{3.1}$$

Where x is the resistance measurement of one of the sensor's channels. Using this formula, we first subtract from each measurement value, the minimum value of the data set to reduce the data offset, then we divide by the total range of sensor's channels resistance values. All resulting data x' are thus in the interval between 0 and 1. Figure 3.2 shows the results of the formula when applied to the data.

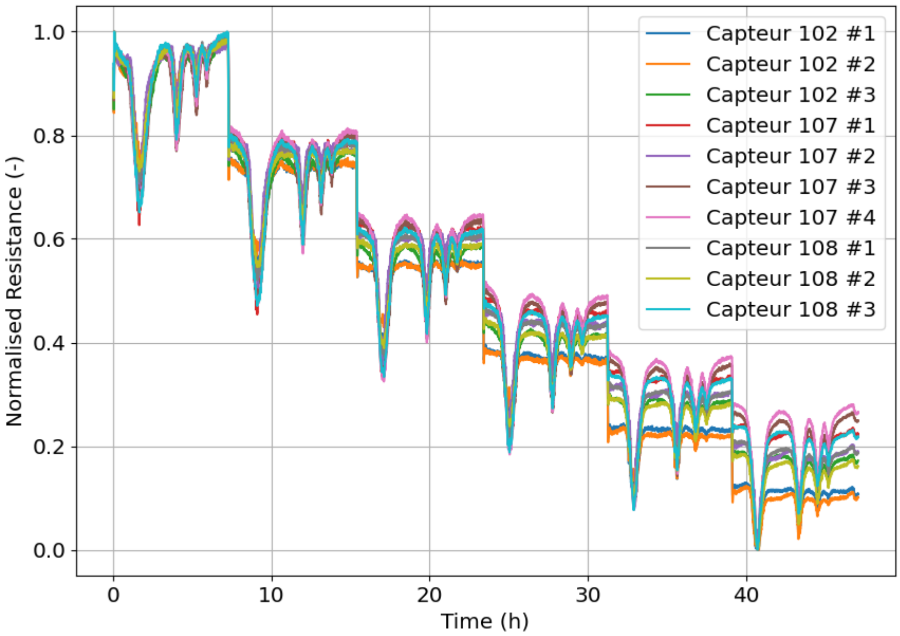

Figure 3.2: Min-max normalization

For high resistors, the resistance values match well. However, for low resistors, there is a shift in the resistance values.

3.1.2 Mean normalization

This second way of normalising is very similar to the first. Instead of subtracting the minimum value from the data, we subtract the average value:

$$x' = \frac{x - \text{mean(x)}}{\text{max(x)} - \text{min(x)}} \tag{3.2}$$

After applying the formula to the sensors resistance values, we obtain the figure 3.3

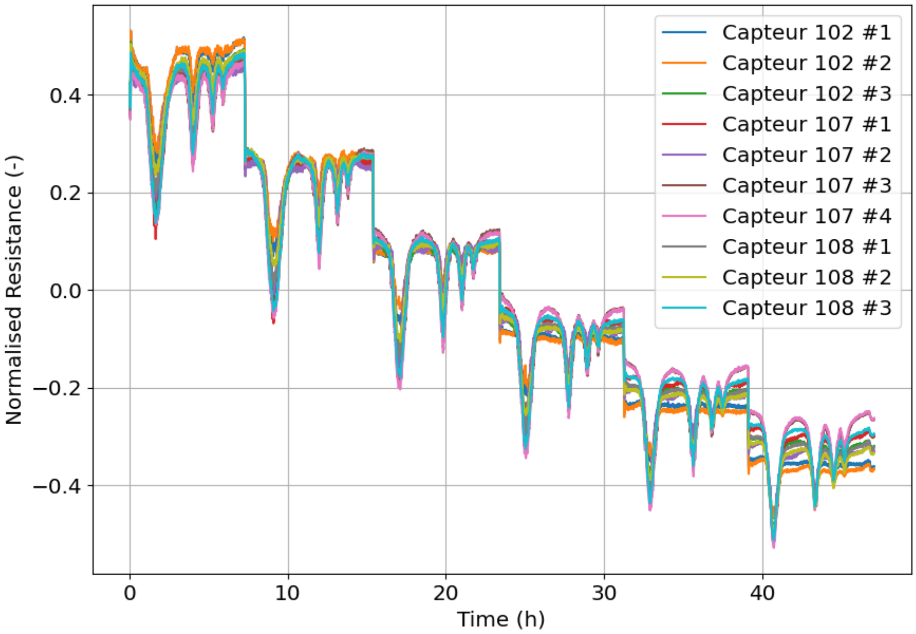

Figure 3.3: Mean normalization

The data are a little closer together, but the gap is still large for low resistances. Subtracting x by the mean and not by the minimum value creates a smaller offset. The average takes into account the whole dataset and not just one (minimum) value of the data.

3.1.3 Standard score

The last standardisation tested is the Standard score. For this standardisation, we use the same formula than for the Mean normalization but we divide by the standard deviation of the dataset in place of the difference between the maximum and minimum value of x. The results x' are again either positive or negative in an interval that varies following the dataset values.

$$x' = \frac{x - \text{mean(x)}}{\sigma(x)} \tag{3.3}$$

This gives us figure 3.4.

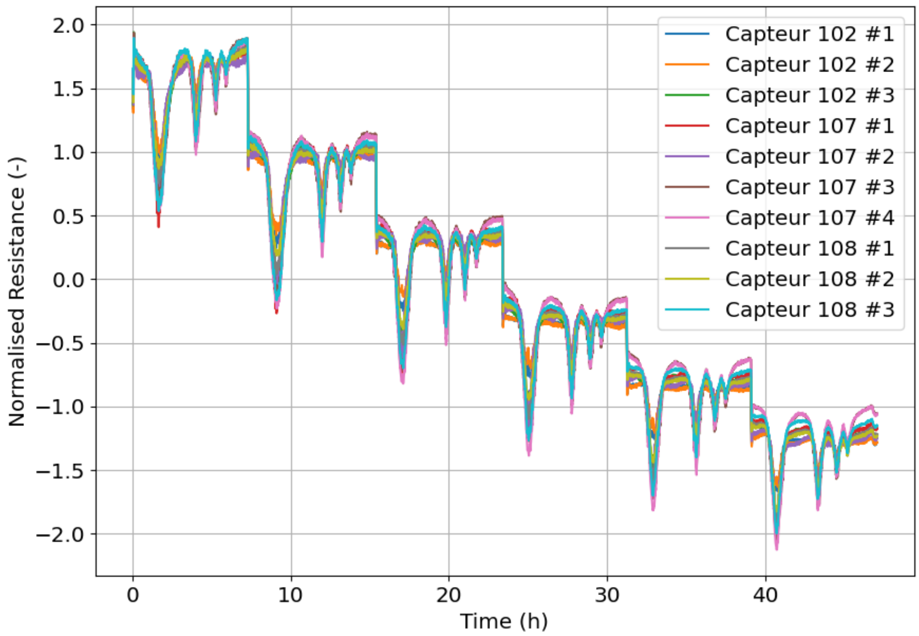

Figure 3.4: Standard score normalisation

The standard score gives the best result. There is yet a small offset between the different data but the offset is almost constant for any level of resistance. This level of standardisation is satisfactory. For the remainder of this thesis, we use thus data normalised by the standard score.

3.2 Filtering

Once the data have been normalised, we now need to filter them to enhance the quality of the information conveyed by the signal. The data comes from 3 measurements: resistance (output), temperature (system state) and humidity (input). Each of these 3 measurements will be filtered differently.

Resistance : For resistance measurements, there is much more ripple than for the other measurements. This can be seen in figure 3.5. We need to determine whether these are normal system response or noise. As we know that the temperature doesn't change and that the relative humidity changes slowly, we conclude that the system response, which depends on the input, also changes slowly. We conclude that our signal is in the low frequency range and that some noise has been added.

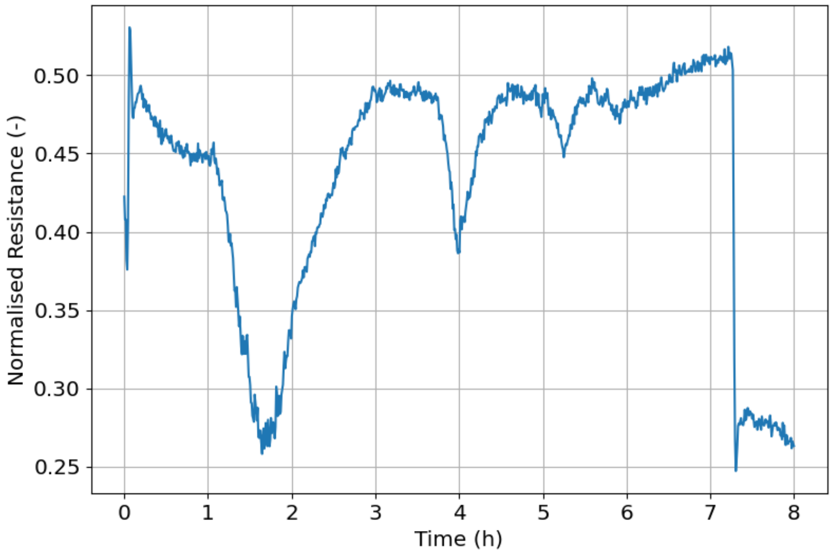

Figure 3.5: Zoom on resistance values with no filtering

Temperature : The temperature is not filtered out. In fact, when the temperature is constant, it doesn't vary more than +/-0.3 degrees Celsius. It will be therefore considered as constant during modelling, and only the average will be used. Consequently, it is not useful to filter it.

Humidity : Humidity is given with a resolution of 1. It does not have a decimal point, as can be seen in figure 3.6. A filter is used to smooth the signal.

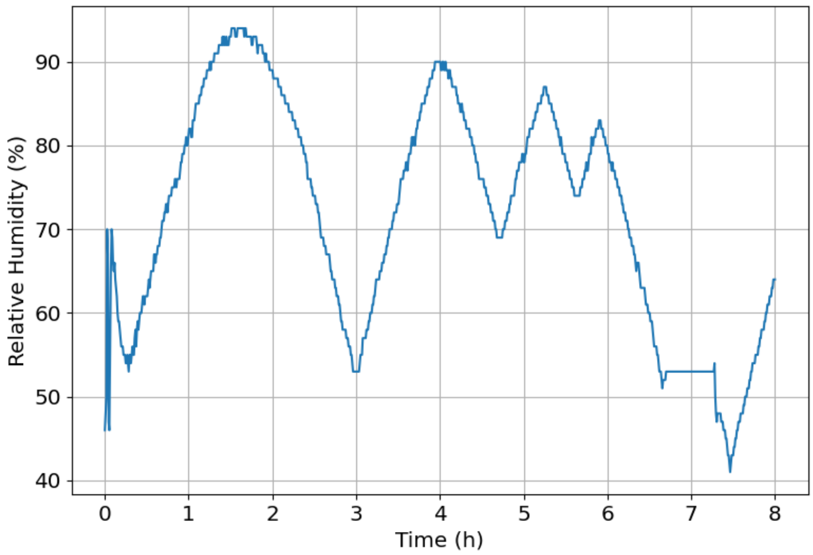

Figure 3.6: Zoom on relative humidity data with no filtering

For the rest of this section, we look at two filter methods and we evaluate the quality of these filters on the experimental data.

3.2.1 Savitzky-Golay filter

The first method is the use of a Savitzky-Golay filter. The Savitzky-Golay filter is a digital filter used to smooth the data. It reduces ripples while maintaining the shape of the signal. The Savitzky-Golay filter behaves like a moving average. For each of the points, a moving average takes the average of a certain number of its neighbouring points.

Instead of taking an average, we take a polynom of degree n over the neighbouring points. A moving average is in fact a specific case of a Savitzky-Golay filter where the degree of the polynom is 1. This filter uses two parameters, the number of neighbouring points and the degree of the polynomial. After trying different parameters, a window of 30 neighbouring points and a polynomial of degree 5 gave the best filter as shown in figure 3.7.

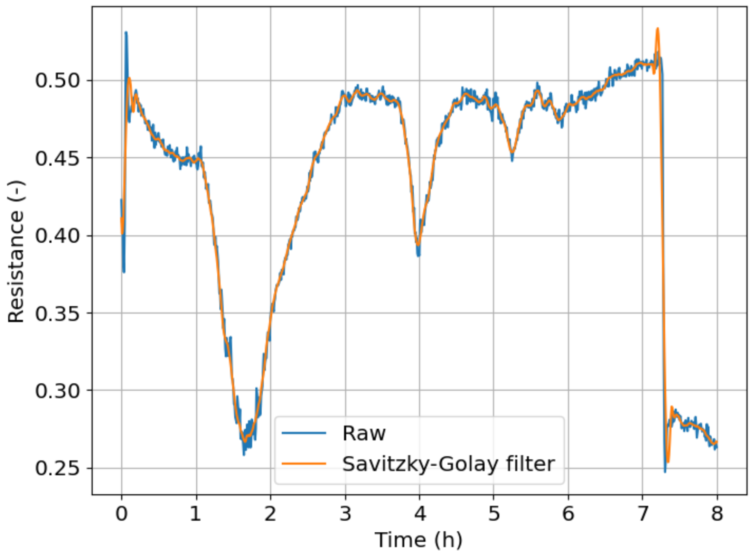

Figure 3.7: Resistance before and after the Savitzky-Golay filter, with the windows w = 30 and the polynom n = 5

And for humidity, we used the same parameters, giving this figure 3.8.

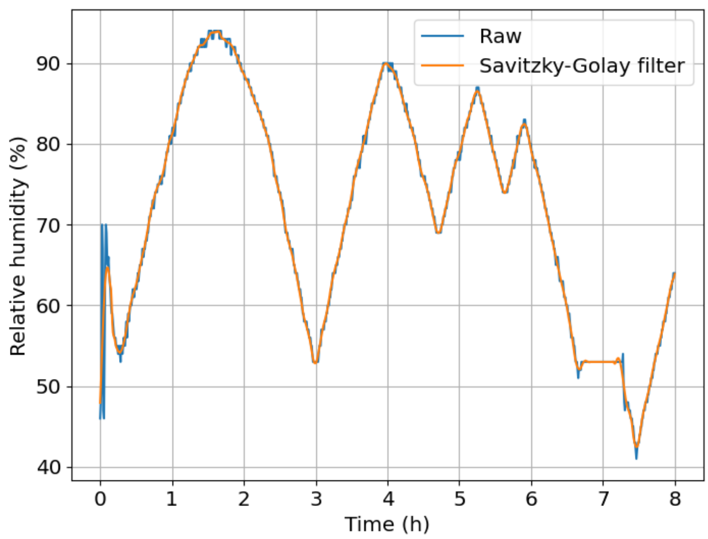

Figure 3.8: Relative humidity before and after the Savitzky-Golay filter, with the windows w = 30 and the polynom n = 5

We want a filter that smoothes the data as much as possible without changing the shape of the filter. In the figure 3.7, there are still ripples on the top of the signal. We'd like something perfectly smooth at the top. To achieve this, we'll look at another method, Wavelets.

3.2.2 Wavelet

Data can also be smoothed using another technique, called Wavelets. Wavelets are a signal processing method that can be used to replace the Fourier transform for analysing complex signals. Unlike the Fourier transform, which uses sines and cosines to represent frequencies, the wavelet uses finite wave functions that start and end at zero. Wavelets can accurately capture local variations in the signal at different frequency scales because of this characteristic.

The ability of wavelets to provide a selective low-pass filter is a key advantage, as it allows only high-frequency components with significant amplitude to be retained. This helps to retain the overall shape of the signal while suppressing the small amplitude variations that can be caused by noise. For the wavelet filter, we used a level 5 decomposition and 16-coefficient Daubechies wavelets ('db8'). The threshold values are different between the two signals. The result of applying the wavelet filter can be seen for resistance in figure 3.9 and relative humidity in figure 3.10. To see the effect of thresholds on coefficients, they are shown in the appendix 6.2.

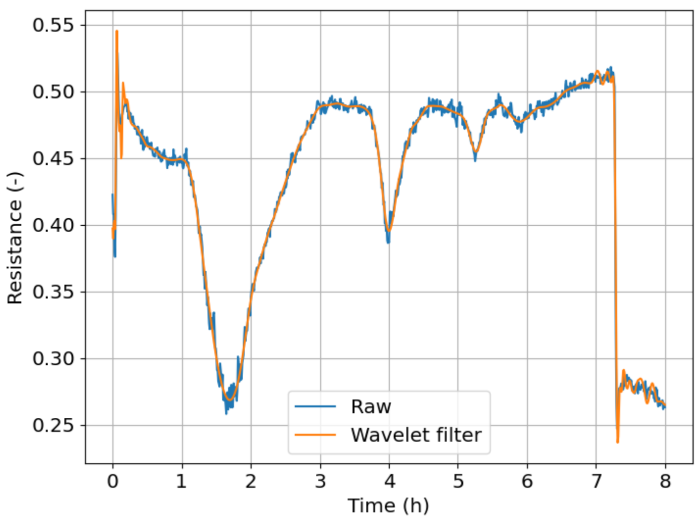

Figure 3.9: Resistance before and after the wavelet filter, with a level 5 of decomposition and array threshold = [0,4,2,30,30]

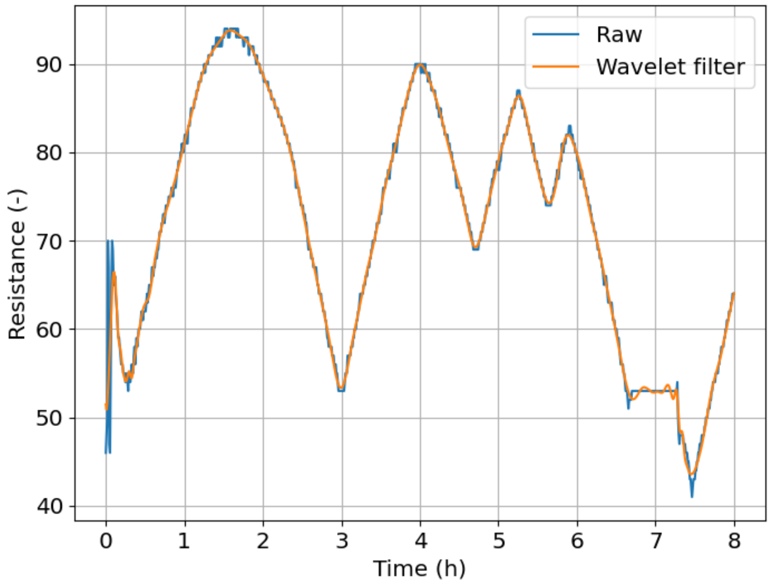

Figure 3.10: Relative humidity before and after the wavelet filter, with a level 5 of decomposition and array threshold = [0,0.05,0.05,0.05,10]

For the resistance, the wavelets give us a very good result. We manage to smooth out the small and large ripples while keeping the original shape of the signal. For humidity, the Savitzky-Golay filter gives better results. In fact, we can see from the figure that the wavelets filter tends to cut the shape of the signal short. Based on this shape criterion, we will use the wavelet filter for channel resistance and the Savitzky-Golay filter for relative humidity.

If we take our figure 2.4 and apply the Wavelet and Savitzky-Golay filters, we get figure 3.11 :

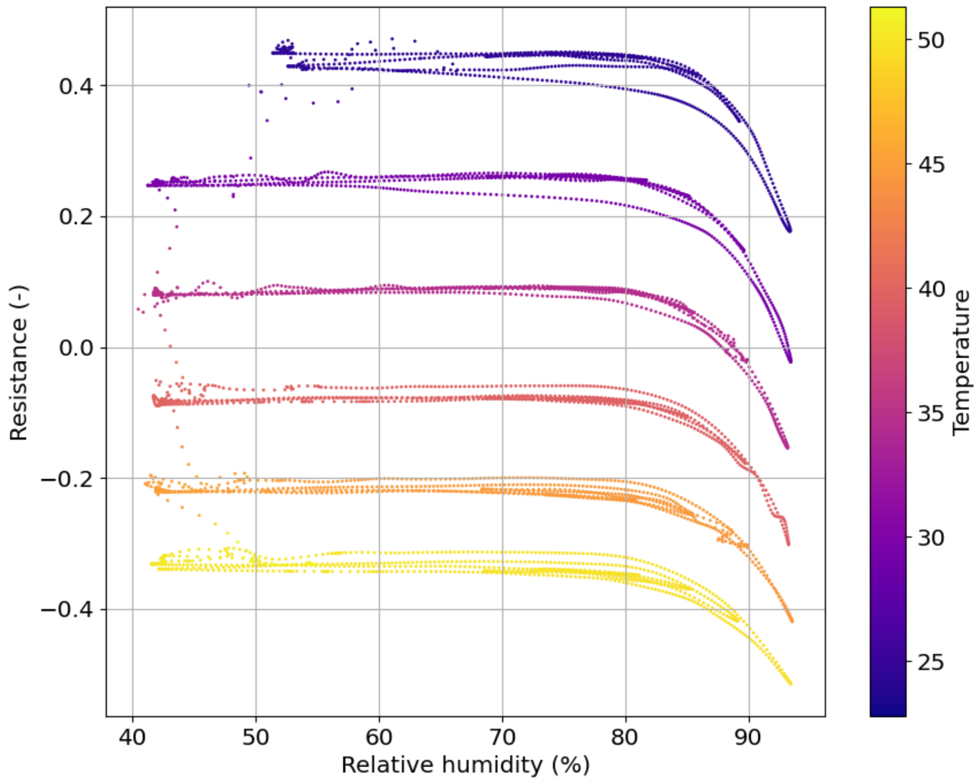

Figure 3.11: Hysteresis effect in the resistance of the micro-captor, filter by the wavelet and the Savitzky-Golay

3.3 Data split

For this last stage, we need to remove the parasitic data. You can see in figure 2.1 and figure 2.2 that the start and end data are very messy. In addition, between each temperature step, the climate chamber has difficulty keeping the relative humidity constant. As the analysis is carried out at constant temperature, the data are separated for each sensor by temperature step.

Chapter 4

Methodology

Up to now we've identified and defined the characteristics of the hysteresis that describes the behaviour of our system. We have also cleaned up the data. We move now to the modelling step. In our case, the physical cause and explanation of the phenomenon is unknown. Indeed, as seen in chapter 2, the physical operation of the sensor is fairly complex and cannot be described in equation form. Therefore we consider it to be a black box. The shape of the hysteresis is known but not its exact expression. For our modelling, a model-driven approach is used for which there are various methods in the literature.

The first model that has been tested is the Prandtl-Inslinskii. This model consists of stacking different linear operators (play and stop operator) which together create a non-linear system. This model is often used in the literature [9][11]. It has the advantage of being invertible, making it possible to improve the control of systems under the effect of hysteresis. After matching the model, it failed to converge towards the curve. In fact, this model can only simulate S-shaped hysteresis as it is designed to work correctly on magnetic hysteresis. This method is thus put aside and the modelling effort concentrates on mathematical function that describe the shape of the hysteresis.

4.1 Sigmoid function

For the second approach, I have tried to describe hysteresis is by mathematical functions. For mathematical expression, the best candidates are sigmoid functions. These curves tend towards a horizontal asymptote at $x = +\infty$ and $x = -\infty$, often between $y = -1$ and $y = 1$ or between $y = 0$ and $y = 1$. They also have an inflection point which is generally at the origin. There are several types of mathematical expression for sigmoids, as shown in figure 4.1.

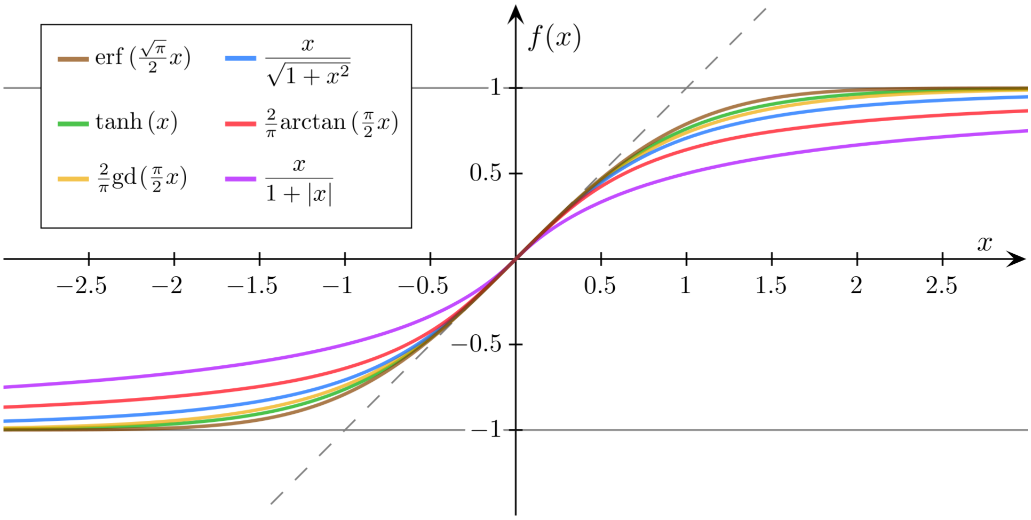

Figure 4.1: Representation of various sigmoids, image borrowed from Wikipedia : `https://en.wikipedia.org/wiki/Sigmoid_function`

4.1.1 Modelisation of Sigmoid

A sigmoid model needs to be selected. The general form of hysteresis is known but its exact form is not. We need a model that can take various amplitudes. For this, the Richardson curve seems a good choice :

$$f(x) = A + \frac{K - A}{(C + Q * e^{-b(x-x_0)})^v} \tag{4.1}$$

where

A is the left asymptote

K and C are parameters for the right asymptote

Q is related to the inflexion point

b is the growth rate

v is symmetric growth parameter

This equation has many parameters. This allows greater freedom of shape for the curve and therefore a better fit. But the problem with too many parameters is the risk of not converging quickly enough toward a solution when fitting.

To make the function fit our problem, the assumptions made in Chapter 2 needs to be applied.

The first assumption A1 is that the resistance changes as a function of the relative humidity and that the temperature is only a parameter of the system :

$$y(h(t)) = A + \frac{K - A}{(C + Q * e^{-b(h(t)-h_0)})^v} \tag{4.2}$$

where

$h(t)$ is the input signal, the relative humidity

h_0 is the shift operator of or model

The next assumption we apply is A4: when x tends towards $-\infty$, $f(t)$ tends towards a horizontal asymptote. This asymptote depends on the temperature $H_{\mathrm{a}}(T)$:

$$y(h(t), T) = H_{\mathrm{a}}(T) + \frac{K - H_{\mathrm{a}}(T)}{(C + Q * e^{-b(h(t)-h_0)})^v} \tag{4.3}$$

The next assumption we consider is A6: $f(t)$ has an oblique asymptote at around 100% relative humidity. This means that the inflection point of the sigmoid must be at 100% relative humidity. To achieve this, the second derivative must be equal to 0 at this point. The first thing to do is to set $x_0 = 100$:

$$y(h(t), T) = H_{\mathrm{a}}(T) + \frac{K - H_{\mathrm{a}}(T)}{(C + Q * e^{-b(h(t)-100)})^v} \tag{4.4}$$

Then we have the second derivative :

$$y''(h(t), T) = b^2 Q v e^{-2b(h(t)-50)} (H - K)(Q e^{-b(h(t)-100)} + C)^{-v-2} (C e^{bh(t)} - Q v e^{100b})$$

$$y''(100, T) = b^2 Q v e^{-100b} (H - K)(Q + C)^{-v-2} (C - Qv) e^{100b} = 0 \tag{4.5}$$

For the second derivative to cancel, either $Q = -C$ or $C = Qv$. In the S-shaped configuration, Q and C are positive. The first solution is therefore not possible. We will use the second one by replacing Q by $\frac{C}{v}$:

$$y(h(t), T) = H_{\mathrm{a}}(T) + \frac{K - H_{\mathrm{a}}(T)}{C^v (1 + \frac{1}{v} * e^{-b(h(t)-100)})^v} \tag{4.6}$$

The problem with this formula is that the parameters K and C have the same role. They both define the value towards which the horizontal asymptote tends in $+\infty$. We want the parameter K to be the value that defined the horizontal asymptote in $+\infty$. We will replace K as a function of L :

$$\lim_{h(t)\to+\infty} y(h(t),T) = H_{\mathrm{a}}(T) + \frac{K - H_{\mathrm{a}}(T)}{C^v} = L \tag{4.7}$$

Which gives us :

$$K = C^v(L - H_{\mathrm{a}}(T)) + H_{\mathrm{a}}(T) \tag{4.8}$$

and in the main equation :

$$y(h(t),T) = H_{\mathrm{a}}(T) + \frac{C^v(L - H_{\mathrm{a}}(T))}{C^v(1 + \frac{1}{v} * e^{-b(h(t)-100)})^v} \tag{4.9}$$

The term C^v cancels out and gives:

$$y(h(t),T) = H_{\mathrm{a}}(T) + \frac{(L - H_{\mathrm{a}}(T))}{(1 + \frac{1}{v} * e^{-b(h(t)-100)})^v} \tag{4.10}$$

The last assumption to take into account for the mathematical model is A7. Our hysteresis has two forms, one when the derivative of humidity is negative and one when it is positive:

$$y(h(t),T,sign(\dot{h}(t))) = \begin{cases} y_1 = H_{\mathrm{a}}(T) + \frac{(L_1 - H_{\mathrm{a}}(T))}{(1+\frac{1}{v_1}*e^{-b_1(h(t)-100)})^{v_1}}, & \text{if } \frac{dh}{dt} >= 0 \\ y_2 = H_{\mathrm{a}}(T) + \frac{(L_2 - H_{\mathrm{a}}(T))}{(1+\frac{1}{v_2}*e^{-b_2(h(t)-100)})^{v_2}}, & \text{if } \frac{dh}{dt} < 0 \end{cases} \tag{4.11}$$

This sigmoid function gives the relationship between the resistance and the relative humidity, the temperature and the sign of the derivative of the relative humidity. We now need to incorporate the memory dependence factor in our system.

4.1.2 Taylor expansion

As stated in Chapter 1, hysteresis is not a mathematical function. We have a function that describes the curve of the hysteresis but now we need an algorithm that simulates the complete hysteresis cycle.

Under the assumption A2, we have that $y(t)$ depends on the past response, the temperature, the relative humidity and the sign of the derivative of relative humidity. The past response needs thus to be integrated into our model. The rest of this section is heavily inspired by the article [5].

Our model is of the rate-independent type A2. Consequently, our sigmoid function depends only on the sign of the derivative and not on the amplitude of the derivative. This allows us to write our problem in this differential form :

$$\frac{dy}{dt} = \frac{dy}{dh}\frac{dh}{dt} \tag{4.12}$$

Where

$\frac{dy(t)}{dt}$ is the time evolution of the resistance,

$\frac{dy}{dh}$ is the slope of the sigmoid curve,

$\frac{dh}{dt}$ is the time evolution of humidity.

In fact, we are still using a rate-independent model because our $\frac{dy}{dh}$ factor does not depend on the signal derivative but only on the value of $h(t)$. The change in resistance as a function of time $\frac{dy(t)}{dt}$ is equal to the change in humidity as a function of time $\frac{dh}{dt}$ along the $\frac{dy}{dh}$ curve.

What is important to know is not the rate of change of the resistance y but the amount of change in the resistance y as a function of a change in humidity. A new assumption based on Maxwell's relations is therefore needed. We consider that our model can be separated into two terms, one that reacts to a change in humidity and one that reacts to a change in temperature :

Assumption 9 *The differentiable model of the hysteresis is expressed in two terms:*

$$dy = \left(\frac{dy}{dh}\right)_T dh + \left(\frac{dy}{dT}\right)_h dT \tag{4.13}$$

In our case, as the temperature is constant, the dT temperature is 0. The term $\left(\frac{dy}{dh}\right)_T$ is therefore the derivative of the sigmoid for a constant temperature. Therefore the following expression :

$$dy = \left(\frac{dy}{dh}\right)_T dh \tag{4.14}$$

The sigmoid curve describes thus the evolution of the resistance as a function of a small change in humidity. For very small shifts, the first derivation of the slope is enough to find the next point. In our case, the smallest known displacement of the relative humidity is 1 %, since the resolution of the relative humidity is 1.

To move along the curve, we need to choose a way of predicting the next point, based on the current relative humidity. In this thesis, we propose to perform a Taylor expansion for the calculation of the next point. Although this Taylor algorithm is not mentioned in the reference literature, it seems to be a good choice for the accuracy of the result. We therefore perform a Taylor expansion around the current relative humidity to predict the next point :

$$\begin{aligned} f(x) &= f(a) + \frac{df(a)}{dx}\frac{(x-a)}{1!} + \frac{df^2(a)}{dx^2}\frac{(x-a)^2}{2!} + ... + \frac{df^n(a)}{dx^n}\frac{(x-a)^n}{n!} \\ &= \sum_{n=0}^{+\infty} \frac{df^n(x-a)}{dx^n}\frac{(x-a)^n}{n!} \end{aligned} \tag{4.15}$$

with $x = h(t)$ and $a = h(t-1)$:

$$\begin{aligned} y(h(t)) &= \sum_{n=0}^{+\infty} \frac{d^n y(h(t-1))}{dh^n(t)}\frac{(h(t)-h(t-1))^n}{n!} = \sum_{n=0}^{+\infty} \frac{d^n y(h(t-1))}{dh^n(t)}\frac{(\Delta h)^n}{n!} \\ &= y(h(t-1)) + y'(h(t-1))\Delta h + y''(h(t-1))\frac{(\Delta h)^2}{2!} \\ &\quad + ... + y^{(n)}(h(t-1))\frac{(\Delta h)^n}{n!} \end{aligned} \tag{4.16}$$

Using a Taylor expansion of a function is used, it's not necessary to apply a chain rule : we are working around the point h(t) and not with the function of time. It would give the same result because, if we did it as a function of time, we would find our humidity value for that time in the second term of our chain rule. For the initial condition, this is the evaluation of the resistance for the initial relative humidity.

For the simulation, the first three derivatives have been taken :

$$y'(h) = be^{-b(h-100)}(L-H)\left(1 + \frac{e^{-b(h-100)}}{v}\right)^{-1-v} \tag{4.17}$$

$$y''(h) = \frac{b^2v^2(e^{b(h-100)} - 1)(H - L)}{\left(1 + \frac{1}{ve^{b(h-100)}}\right)^v (1 + ve^{b(h-100)})^2} \tag{4.18}$$

$$y'''(h) = \frac{b^3(L - H)v^2 \left(v + ve^{2b(h-100)} - (3v + 1)e^{b(h-100)}\right)}{\left(\left(\frac{e^{-b(h-100)}}{v} + 1\right)^v\right)(1 + ve^{b(h-100)})^3} \tag{4.19}$$

The 4th derivative becomes too complex and adds very little precision. Calculating the accuracy and error depends on the point at which the approximation is applied. A visual assessment should be enough to confirm this.

At this point, the resistance of the past $y(t-1)$ is integrated in our model. To be complete, the function of the forward path y_1 and the function of the return path y_2 needs to be matched at the change of sign of $\frac{dh(t)}{dt}$.

4.1.3 Matching

The last part of the model is the crossing of the two functions. In fact, when taking the return path, the second curve y_2 must start again from the point where the forward function y_1 arrived. As the parameters b_2 and v_2 are kept for matching the curve to the data. The parameter L_2 is used for forcing the crossing :

$$y_1(h_{cross}) = y_2(h_{cross})$$

$$H_a(T) + \frac{(L_1 - H_a(T))}{(1 + \frac{1}{v_1} * e^{-b_1(h_{cross}-100)})^{v_1}} = H_a(T) + \frac{(L_2 - H_a(T))}{(1 + \frac{1}{v_2} * e^{-b_2(h_{cross}-100)})^{v_2}}$$

With $A_1 = (1 + \frac{1}{v_1} * e^{-b_1(h_{cross}-100)})^{v_1}$ and $A_2 = (1 + \frac{1}{v_2} * e^{-b_2(h_{cross}-100)})^{v_2}$,

$$\begin{aligned} \frac{(L_1 - H_a(T))}{A_1} &= \frac{(L_2 - H_a(T))}{A_2} \\ \implies L_2 &= L_1\left(\frac{A_2}{A_1}\right) + \left(1 - \frac{A_2}{A_1}\right) H_a(T) \end{aligned} \tag{4.20}$$

L_2 is replaced in the equation 4.11.

4.2 description of the hysteresis model

We'll see how our model responds to a simple function before fitting it to the data. For the first test, a sinusoidal signal 4.2 with a period of 4800 seconds and a triangular signal 4.3 with a period of 9600 seconds are used. Both signals start at a relative humidity of 20%. The relative humidity rises to a maximum of 95% and then falls back to the starting value.

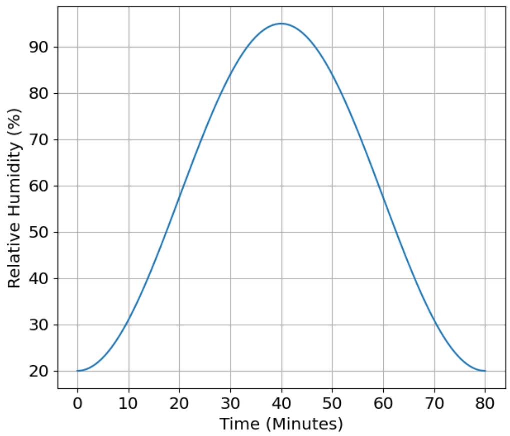

Figure 4.2: Sine wave

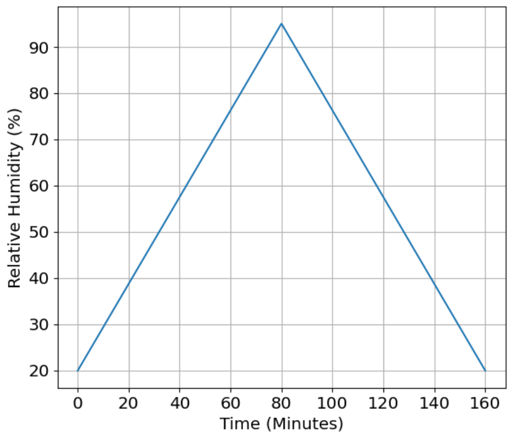

Figure 4.3: Triangle wave

Figure 4.4: Two input signals with different frequencies, a sinusoidal signal with a period of 4800 s and a triangular signal with a period of 9600 s

The result of the algorithm with the two signals 4.4 gives the figure 4.5. In blue we have the result of the algorithm for the sine wave function 4.2 and in dotted orange the result for the triangle wave function 4.3. It doesn't matter what the shape or frequency of the input signal is, only the amplitude has an impact on the result. In terms of accuracy, the figure 4.6 shows a zoom on the start and return of the hysteresis. The accuracy is of 0.1%. This deviation is due to the Taylor series approximation but the precision is good and justifies taking only the first 3 derivatives for the Taylor series.

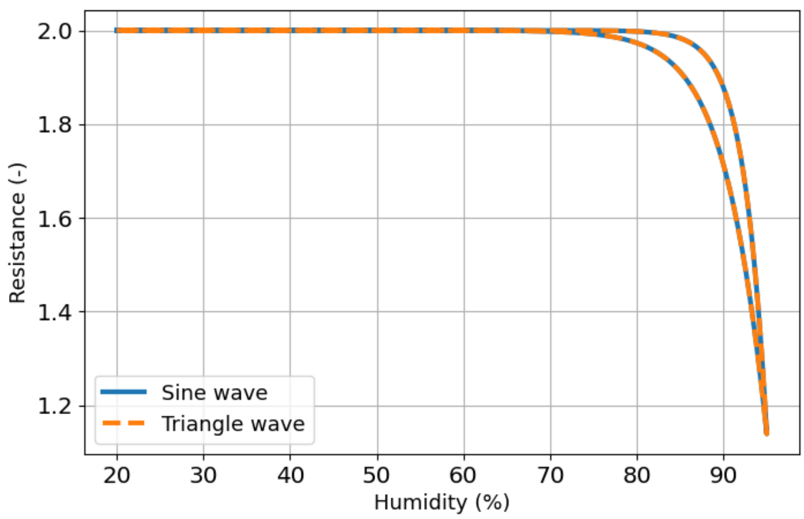

Figure 4.5: Result of the algorithm for two different input signals with $H = 2$,$L = -6$,$b_1 = 0.5$,$b_2 = 0.3$,$v_1 = 0.8$,$v_2 = 0.8$

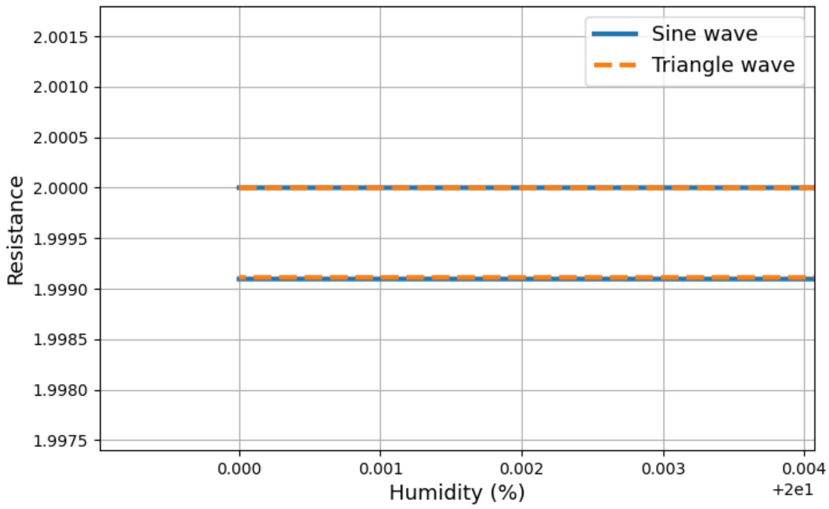

Figure 4.6: Zoom in on the start and return of hysteresis

Finally, for the last test, an input signal similar to that in Experiment 2 (see figure 4.7) is used. Figure 4.8 and Figure 4.9 show the results of our model for this input signal. This corresponds to the analysis carried out in Chapter 2. The shift in hysteresis at low relative humidity is not due to the accuracy of the approximation but to the speed of convergence of the return path towards the horizontal asymptote. In the next chapter, we apply our model to the experimental data and determine the parameters of our model.

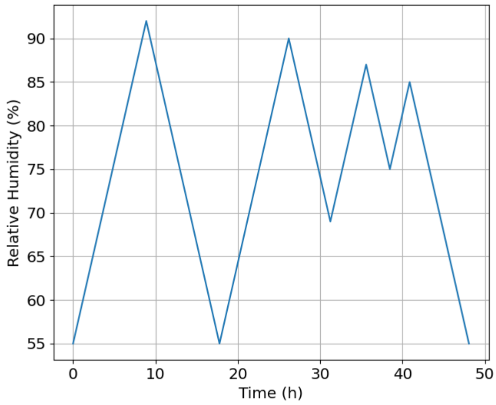

Figure 4.7: Humidity signal profile, same as experiment 2

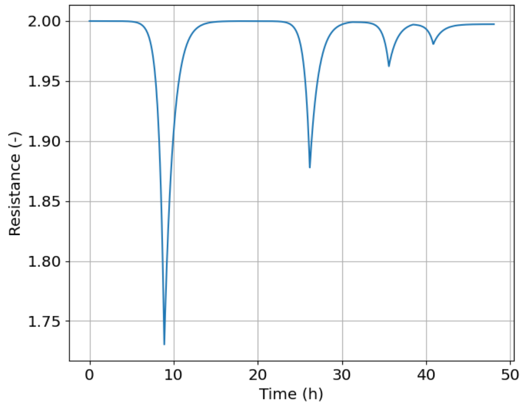

Figure 4.8: Change in resistance as a function of time

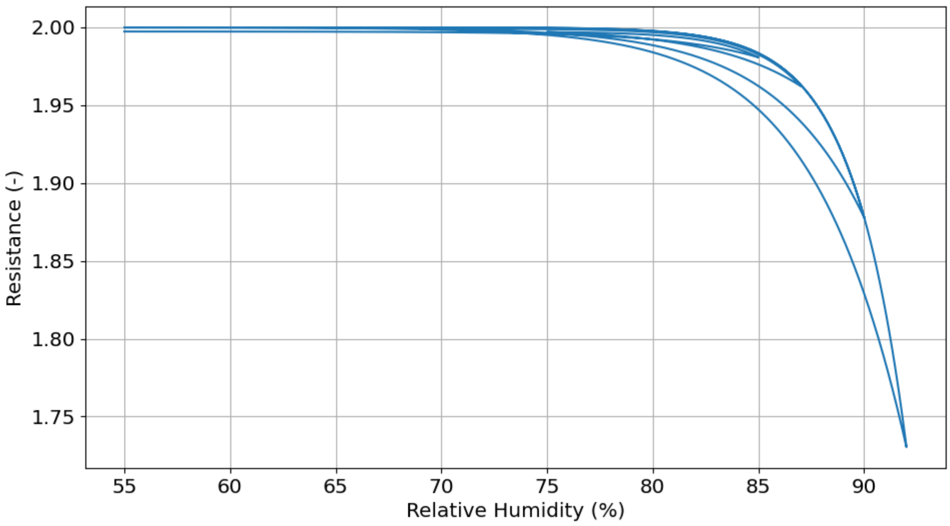

Figure 4.9: Model hysteresis for input signal 4.7 with $H = 2$,$L = -6$,$b_1 = 0.5$,$b_2 = 0.3$,$v_1 = 0.8$,$v_2 = 0.8$

Chapter 5

Result

The mathematical model being built, we need to determine now the parameters of the model. To fit the model to the data, the Levenberg-Marquardt algorithm is used. This algorithm minimises the least squares of non-linear problems [33] which is perfectly suited to this problem.

Concerning the data, we have two experiments results. The first with a step change in humidity and the second with a continuous change in humidity. Due to the gradual change in humidity in the second experiment, the resistance changes continuously also. For training the model, the data from experiment 2 are thus easier to use because, with continuity, the model is easier to fit to the data. For this experiment 2, we have 6 temperature levels for 10 sensors. This gives 60 sub-sets of data.

5.1 Parametrization

The first results can be seen in figure 5.1 and figure 5.2. The first figure shows the best result obtained, so with the smallest mean squared error (MSE) ($Err = 0.144$) and the second figure shows the worst result obtained with the largest MSE ($Err = 5.12$).

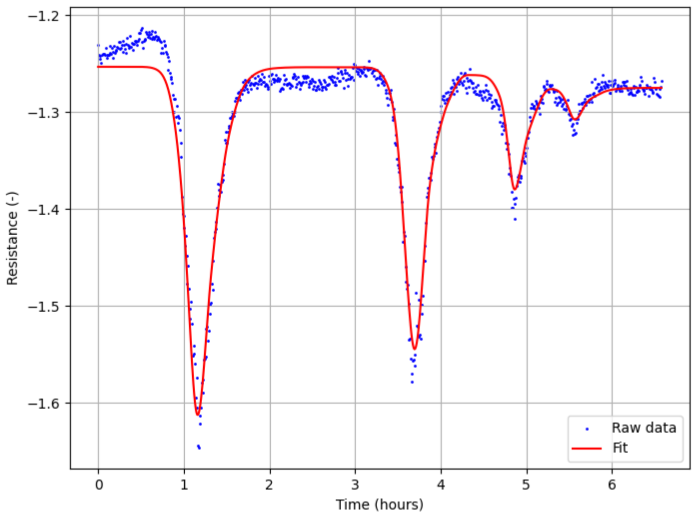

Figure 5.1: Best fit of the hysteresis model ($channel$ = 102-33-1, $T = 49.789°C$, $H = -1.253$,$L = -4.416$, $b_1 = 0.098$, $b_2 = 0.165$, $v_1 = 8.035$,$v_2 = 1.123$) with an error of $2.5 * 10^{-5}$ (MSE)

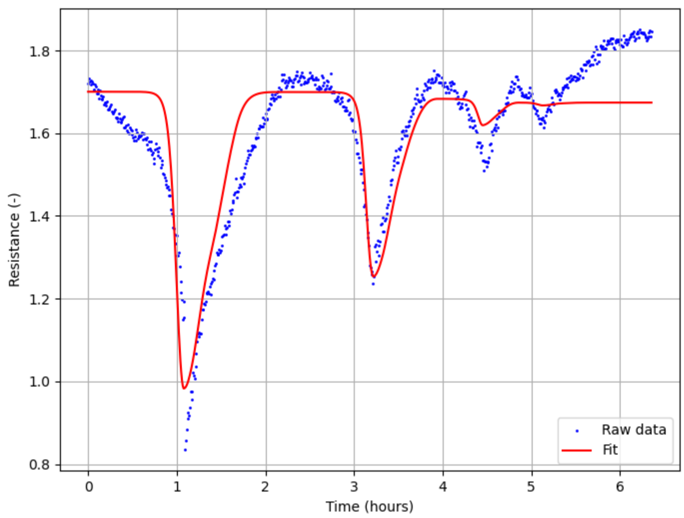

Figure 5.2: Worst fit of the hysteresis model ($channel$ = 102-33-3, $T = 24.315°C$, $H = -1.7$,$L = -147.626$, $b_1 = 1.717$, $b_2 = 0.055$, $v_1 = 0.313$,$v_2 = 563.642$) with an error of $0.97 * 10^{-3}$ (MSE)

To determine the influence of the parameters in the sigmoid equation, the relations between them are identified by the correlation matrix 5.3.

Figure 5.3: Correlation matrix of the parameters T, Delta Y, Err and the model coefficients

where

T is the temperature (mean per split)

ΔY is the spread between the largest and smallest resistance values.

H, L, b_1, b_2, v_1, v_2 are parameter of the model

Err is the sum of square error of the model on the filtered data

This matrix shows the links between the different parameters and state variables of the model. The strongest link is between the temperature and the parameter $H_\mathrm{a}(T)$. Indeed, the variation of the parameter $H_\mathrm{a}(T)$ as a function of the temperature is shown in the figure 5.4

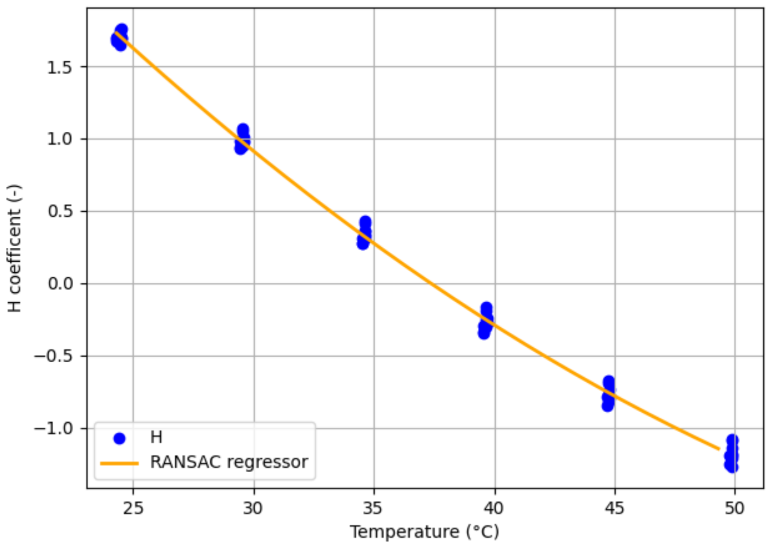

Figure 5.4: RANSAC approximation of the coefficient $H_\mathrm{a}(T)$

This relationship is not exactly linear, contrary to what is supposed in A4. We apply the RANSAC (Random sample consensus) method to approximate our function. The RANSAC method is used because it approximates a function on the closest points and ignores the most distant points (i.e. the outliners that are excluded) [34]. It is a non-deterministic alogrithm and needs to be rerun several times until a satisfactory approximation is obtained. In our case, there are no outliners between $H_\mathrm{a}(T)$ and the temperature. The following relationship is found :

$$H_\mathrm{a}(T) = 0.00147T^2 - 0.223T + 6.2845 \tag{5.1}$$

This approximation by a quadratic function only works for the interior values of the estimate. In fact, the true function of $H_\mathrm{a}(T)$ is of the form $\frac{1}{x^2}$. A simple quadratic function is used in this thesis because a more precise function requires a wider range of temperatures than the one used in the experiments.

In the correlation matrix above, two other major correlations are observed : one between the temperature and the error and one between the temperature and the factor b_1. As far as the error is concerned, the figure 5.5 shows that the error is large for the low temperatures and even larger for the lowest temperatures. Determining the cause is not straightforward, as we don't know whether it's the model that doesn't work very well at low temperatures or whether the data is of poorer quality at low temperatures. If we compare figure 5.2 and figure 5.1 which are respectively showing data obtained at $T = 24.315°C$ and $T = 49.789°C$, there are more variation in the data of 5.2. But it is also known that the MSE of the result of figure 5.2 is the worst one.

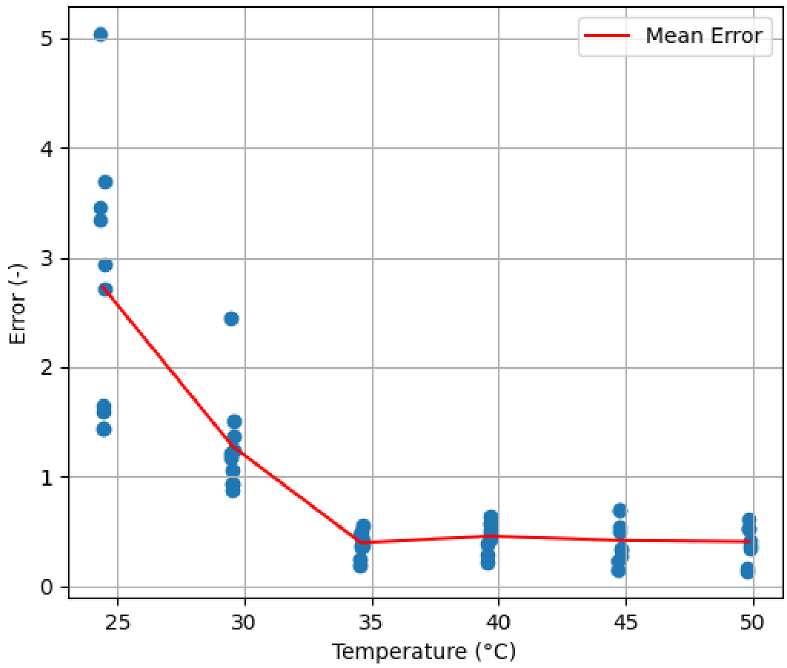

Figure 5.5: Sum of square error of the model fit to the data for each temperature

The second correlation is between temperature and the coefficient b_1. In the correlation matrix, this parameter b_1 is also correlated with $H_a(T)$, which is normal because both are linked by temperature. Figure 5.6 shows the coefficients b_1 as a function of temperature and the original channel. This relationship is less discernible. Indeed, for certain channels, the b_1 coefficient is quite volatile. Excluding the extreme values, only the values of the b_1 coefficients between 0.7 and

2.0 are kept. The figure 5.7 shows the results of the application of the RANSAC algorithm with this range of values. The following relationship for the coefficient b_1 is then deducted:

$$b_1(T) = 0.000778T^2 - 0.087T + 3.386 \tag{5.2}$$

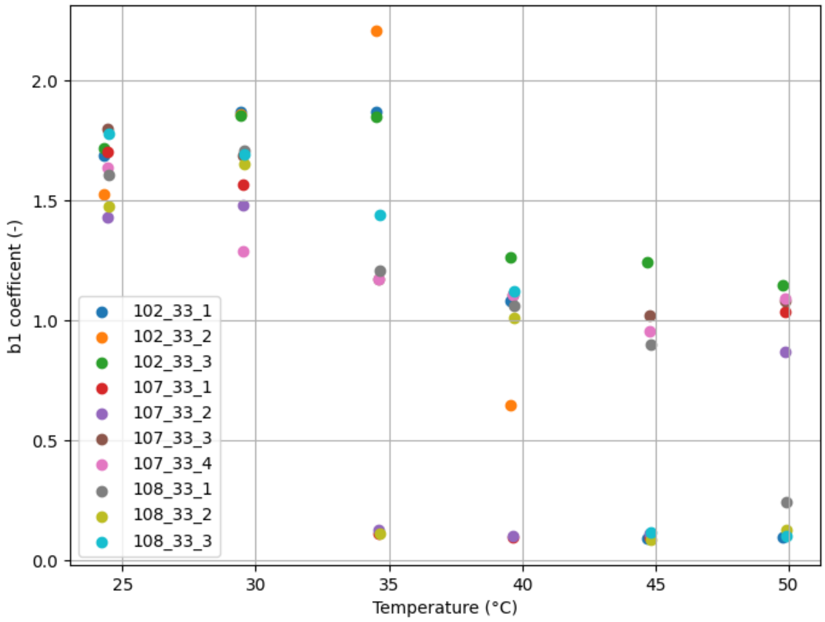

Figure 5.6: Coefficient b_1 for each channel and temperature

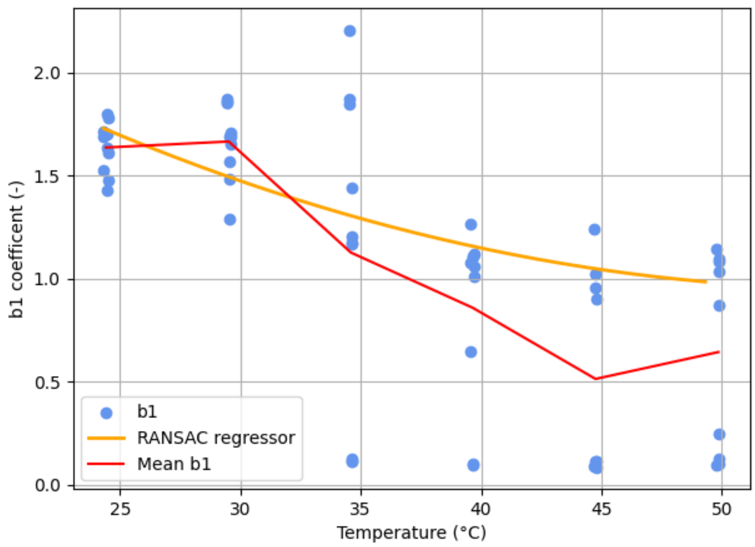

Figure 5.7: Average and RANSAC approximation of b_1 coefficients

Next, I decided to re-run the model while imposing the value of the coefficient b_1 following the formula 5.2 for reducing its volatility. $H_a(T)$ is not fixed because it is stable and fixing it could prevent a better solution. Imposing the coefficient b_1 increases the error when fitting the model, as shown in figure 5.8.

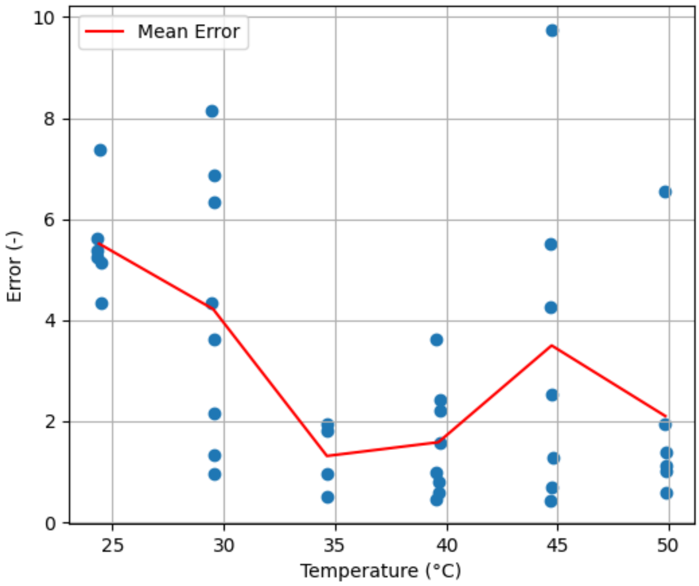

Figure 5.8: Sum square error of the model fit to the data for each temperature for the re-run

For the rest of the parameterization, all the fits with an MSE error greater than 10 are removed. The number of data sub-sets decreases then from 60 to 39.

A new correlation matrix is also obtained and shown in figure 5.9.

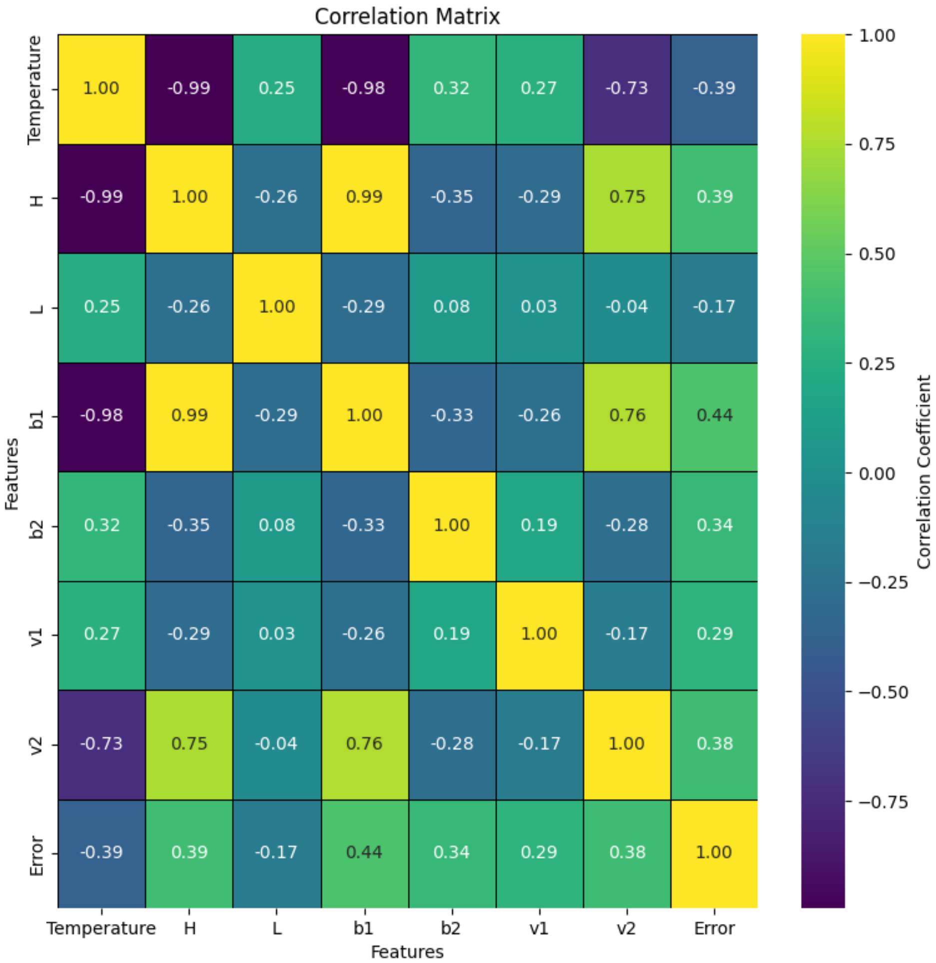

Figure 5.9: Correlation matrix of the parameters T, Delta Y, Err and the model coefficients for the re-run

On this matrix, a significant relationship between v_2 and the temperature appears. The variation of v_2 as a function of the temperature is shown on figure 5.10.

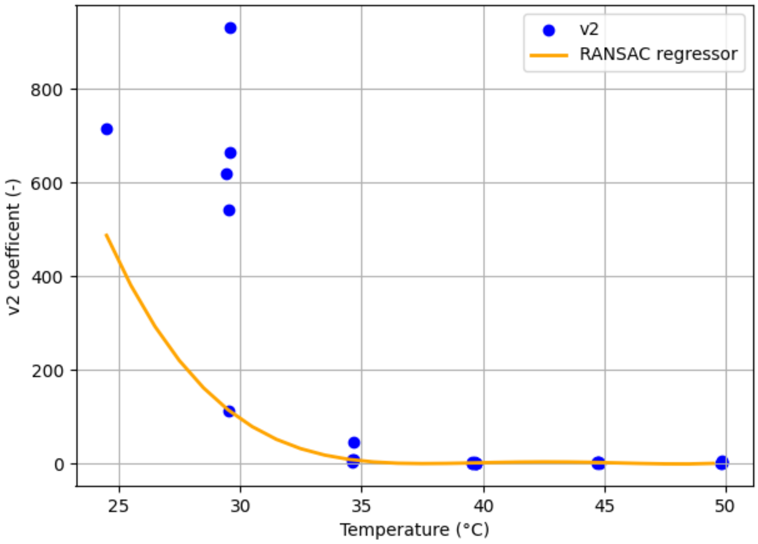

Figure 5.10: RANSAC approximation of the coefficient v_2

In the same way as above, the RANSAC algorithm is applied for finding a correct fit. A polynomial of degree 4 was chosen for a better representation of the curve, following the formula :

$$v_2(T) = 0.00517T^4 - 0.885T^3 + 56.499T^2 - 1595.089T + 16802.37 \tag{5.3}$$

The problem of this function is that it is a polynom that can variate unexpectedly out of the considered interval of temperature . The shape of the curve is a decreasing exponential. A new fit of this type gives the following formula that is more exact:

$$v_2(T) = e^{-0.37*(T-40)} + 2.5 \tag{5.4}$$

The same process is applied to all other parameters of the model.

For v_1 the result is shown in figure 5.11.

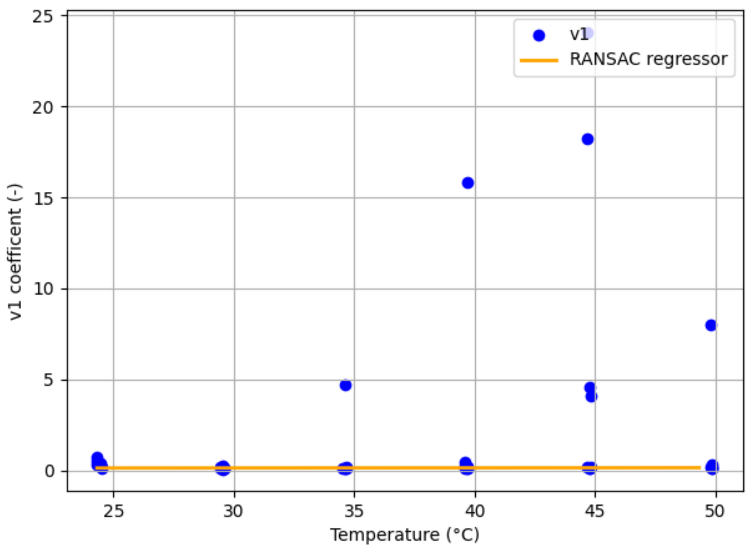

Figure 5.11: RANSAC approximation of the coefficient v_1

And the following relationship is found:

$$v_1(T) = 0.00278T + 0.0352 \tag{5.5}$$

For L, the result is shown in figure 5.12 :

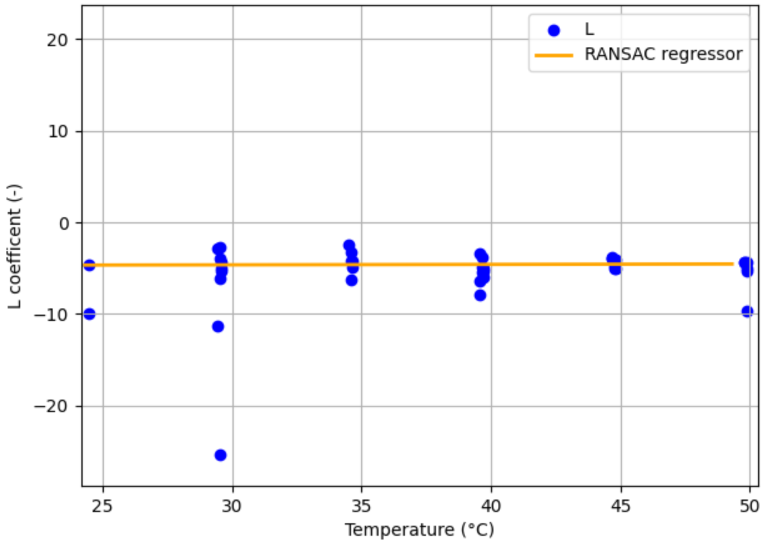

Figure 5.12: RANSAC approximation of the coefficient L

And the following relationship is found:

$$L = -4.772 \tag{5.6}$$

And finally for b_2, the result is shown in figure 5.13.

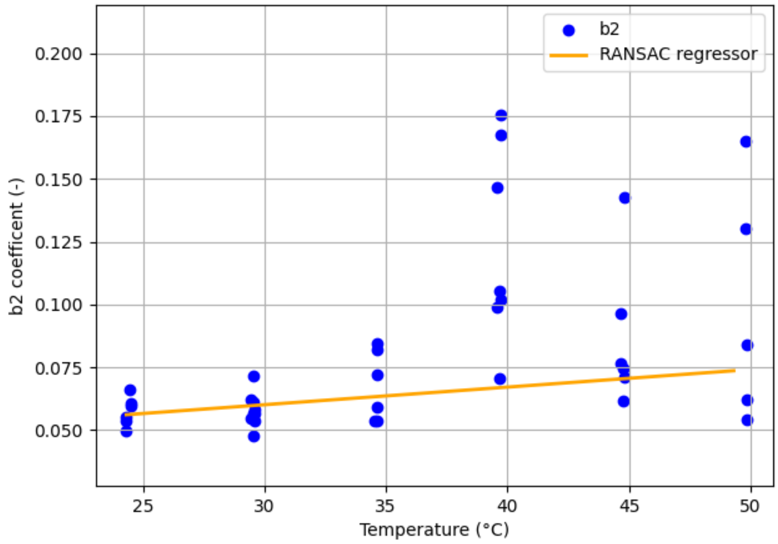

Figure 5.13: RANSAC approximation of the coefficient b_2

And the following relationship is found:

$$b_2(T) = 0.00067T + 0.039 \tag{5.7}$$

5.2 Model confirmation

Finally, we analyse the reaction of the model for a complete humidity signal, for the 6 temperature steps. This implies that we are no longer temperature invariant and that we need to modify our model slightly. We return to equation 4.13. For the term that changes as a function of temperature, we replace it with the function $H_\mathrm{a}(T)$:

$$dy = \left(\frac{dy}{dh}\right)_T dh + H_\mathrm{a}(T) \tag{5.8}$$

The term $\frac{dy}{dh}$ which is expressed by the Taylor expansion remains the same except that the initial condition is no longer the resistance but the difference between the measured resistance and $H_\mathrm{a}(T)$.

The model being complete, the figure 5.14 shows the evolution of the model for the entire humidity signal from experiment 2. Overall, the model's response matches correctly the shape of the data. It conforms to expectations.

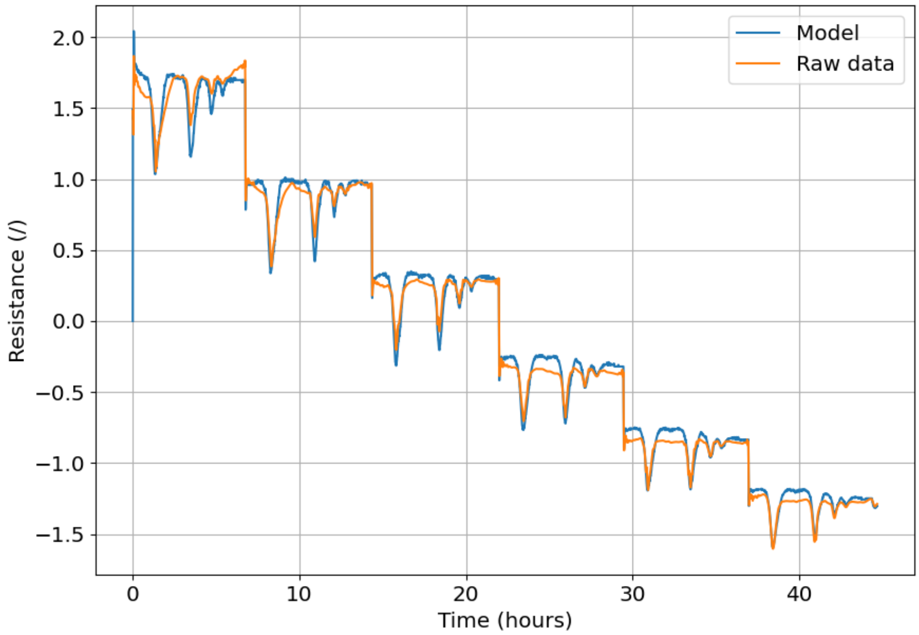

Figure 5.14: Result of the model for the relative humidity of experiment 2 and a channel resistance signal during this one

In figure 5.15 the difference between the response of our model and the raw micro-sensor data, is plotted. The MSE of has a value of 0.0769. There are still a few small peaks but the signal remains close to 0 overall. This is convincing and validates our model.

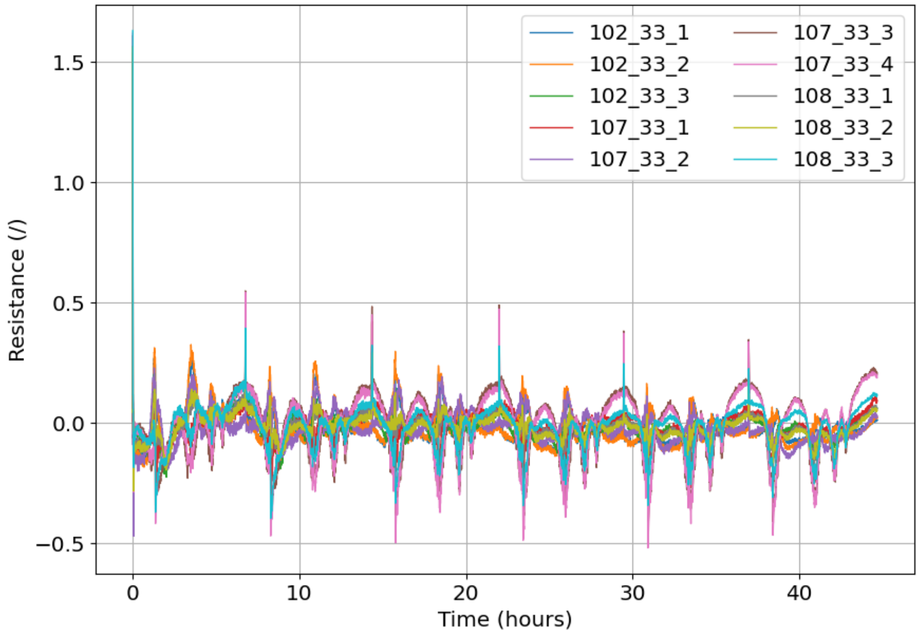

Figure 5.15: Subtraction of the model from all the resistance signals in experiment 1

To complete the validation of our model, our model is applied on the humidity values of experiment 1 and compared with the raw micro-sensor data of this experiment. The evolution of the resistance value can be seen in figure 5.16.

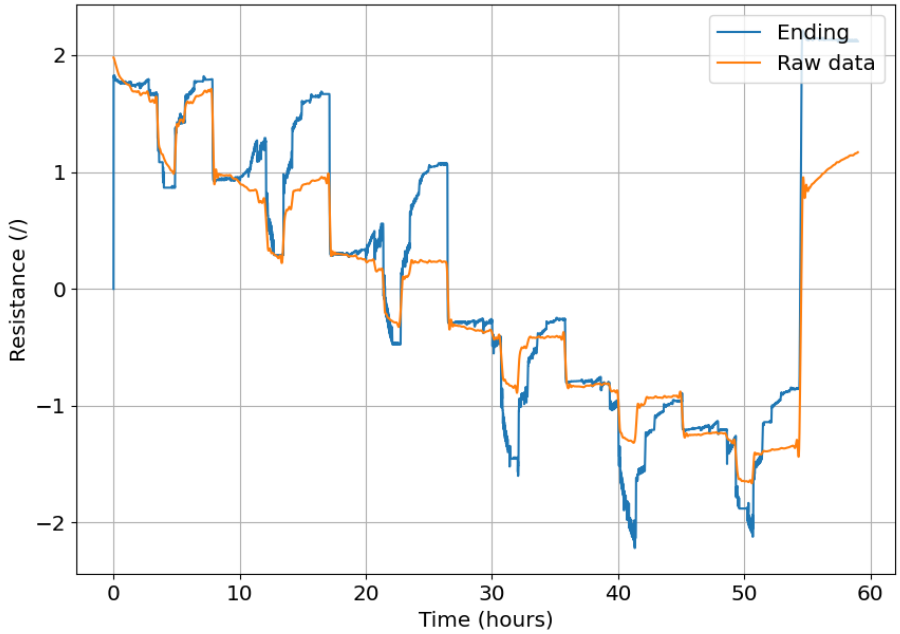

Figure 5.16: Result of the model for the relative humidity of experiment 1 and a channel resistance signal during this one

To obtain this result, the relation for v_1 has been changed to :

$$v_1(T) = 0.00034 * T + 0.0842 \tag{5.9}$$

This shows that the model lacks robustness, probably because of the low number of data sets and the diversity of the signal between the two experiments. The model works well for low temperatures and less so for high temperatures. However, the model can fit correctly the curves.
Finally, the difference between the model result and the raw data is shown on figure :

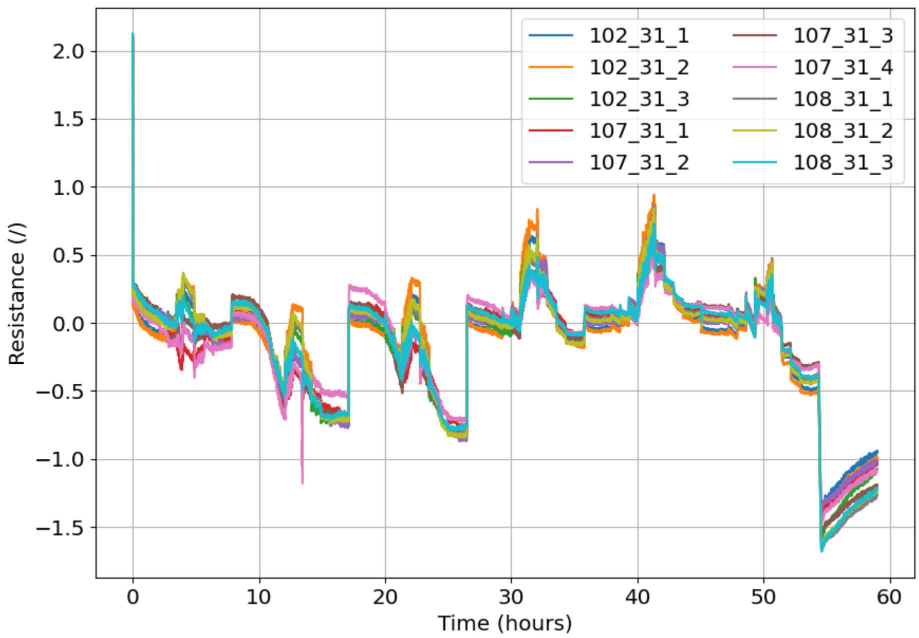

Figure 5.17: Subtraction of the model from all the resistance signals in experiment 1

Chapter 6

Discussion

The hysteresis effect has been analysed and modelled even if the parameterization is not yet complete. Indeed, more experiments than realized were planned originally. This is due to issues with the climatic chamber in which the experiments are conducted. More experiments data sets would have allowed to better determine the behaviour of certain coefficients in the model and to improve the robustness of the model.

The special feature of this thesis is the use of a Taylor expansion to simulate a rate-dependent hysteresis. As the sigmoid curve describes the path of the hysteresis, we follow this curve with small approximate steps. It offers a simple and efficient way for matching the experiments data. However, we must take care of a potential inconvenient when, for many small relative humidity steps, the model could accumulate inaccuracy. This has not been met in our thesis up to now.

6.1 Assumption

In this section, the efficiency and value of the assumptions are evaluated:

A1 : The assumption that the temperature is time invariant was useful for modelling the hysteresis curve even if it is finally out of date. Indeed, under the new assumption 9 and in the model used for the section 5.2 our model is no longer temperature invariant.

A2 : To find out whether our model is Rate-Independent or Rate-Dependent, we need to carry out experiments with variations in relative humidity of different frequencies. It was planned to carry out experiments but the experiments data sets are not available for now.

A3 : To find out if there is degradation, we also need to do an experiment with a constant temperature and relative humidity in the climate chamber. This experiment was also planned but not available for now.

A4 : The hypothesis that the horizontal asymptote H_a depends on temperature is verified by the result in Figure 5.14. However, the relationship with temperature is not linear but quadratic. The best approximation for this function is a decreasing exponential or a function of the form $\frac{1}{x^2}$.

A5 : The decrease point is difficult to calculate. Indeed, with the lack of precision in the coefficients equations, this point is not precise enough. A more robust model would be needed to confirm this hypothesis.

A6 : The assumption that hysteresis is flat at 100% relative humidity was useful for defining and constraining the mathematical model. It could plunge exponentially or tend towards a vertical asymptote at 100% relative humidity. An experiment would be needed to verify the truth of this hypothesis, but it would be complicated as reaching 100% relative humidity in a climate chamber is almost impossible. The one used in our lab is limited to 95%.

A7 : The fact that our hysteresis is expressed by two curves, a return curve and a forward curve, is worth checking. We have different coefficients for the functions y_1 and y_2. One avenue to explore is to use other types of function. For high temperatures, the return path is quite slow when changing resistance, as can be seen in figure 5.2. Choosing a different function for each way (upward and downward) will also allow more precision in the slope of the return path.

A8 : This assumption which mentions that the absolute difference between the raw data and the model must be equal to 0 is rather an objective. This is respected and demonstrated in the section 5.2.

A9 : The expression in two terms is correct and used to the end. For the term $\frac{dy}{dh}$, it's our Taylor expression and for the term $\frac{dy}{dT}$ it's the derivative along the curve $H_a(T)$ as expressed on the equation 5.8 For the temperature term, new experiments would allow to be more precise in the approximation of the H_a curve.

6.2 Further research

Several areas for improvement were not part of the scope of this thesis and can be considered as way to enrich and improve the model:

- **Data** As mentioned above, increasing the amount of data will increase the robustness of the model. In addition, more experience with different relative humidity and temperature changes will improve also the model. However, we are limited by the number of experiments. The experiments take a long time to run (over 40 hours) but a limited number (10-12) would greatly increase the robustness of the model.

- **Other Sigmoid function**

  During the thesis, only one sigmoid was used. As mentioned above for the assumption 7 , we could use other sigmoid models as well as other functions and evaluate their performance.

- **Machine Learning**

  The machine learning track could be interesting, more and more scientific articles use machine learning algorithms to analyse and simulate hysteresis as seen in section 1.3.3 . If we manage to accumulate a lot of data, this could be a very interesting avenue.

- **Memristor**

  The hysteresis analysed in this brief is pinched. A pinched hysteresis effect is also observed in Memristors. The advantage is that the differential equations are known for these [28]. We could adapt them and test them on our case.

,

Conclusion

This thesis explored the analysis and correction of the hysteresis effect in gas micro-sensors, a major challenge in the field of measurement and control systems. Hysteresis, as a non-linear phenomenon, creates significant difficulties for modelling and predicting system behaviour, particularly when accuracy is essential.

In addressing this problem, we have developed and implemented robust methods for the identification, modelling and mitigation of hysteresis.'

The quality of the data used for modelling has been improved by the use of data processing techniques:

- Standard score normalisation,
- Wavelet and Savitzky-Golay filtering.

A significant reduction in the hysteresis effect has been achieved by the application of modelling approaches:

- Richardson type of sigmoid,
- Taylor expansion for the simulation of consecutive values.

The result is a good fit of the model on the experiment data with a mean square error (MSE) of 0.074 on the training data.

The results obtained demonstrate the effectiveness of the proposed hysteresis compensation methodology. This approach is not only applicable to gas microsensors, but can also be generalised to other types of sensors and applications, opening up new prospects for improving the accuracy of measurement systems in various fields.

However, further work is needed to confirm the robustness and generalization of these methods under a variety of conditions and with different types of sensors. Further research in this area could include the exploration of new modelling techniques based on machine learning and artificial intelligence, which could offer even better solutions for hysteresis compensation.

In conclusion, this research makes a contribution to the understanding and correction of the hysteresis effect in gas microsensors, offering practical and effective solutions for improving the accuracy and reliability of measurement systems. Future developments in this important area of electromechanical engineering are identified for improving yet the acuracy and precision.

Bibliography

[1] Britannica, T. Editors of Encyclopaedia. "hysteresis." Encyclopedia Britannica, April 22, 2024.`https://www.britannica.com/science/hysteresis`.

[2] A. Visintin, "Differential Models of Hysteresis", 1994, *Applied Mathematical Sciences*, vol. 111,Springer, Berlin, Heidelberg

[3] Tianyu Wang, Mohammad Noori, Wael A. Altabey, Zhishen Wu, Ramin Ghiasi, Sin-Chi Kuok, Ahmed Silik, Nabeel S.D. Farhan, Vasilis Sarhosis, Ehsan Noroozinejad Farsangi, 2023, "From model-driven to data-driven: A review of hysteresis modeling in structural and mechanical systems", *Mechanical Systems and Signal Processing*, vol 204, 110785, [Online] Available : `https://www.sciencedirect.com/science/article/pii/S0888327023006933`

[4] "Magnetic Hysteresis", *Electronics Tutorials*, [Online] Available : `https://www.electronics-tutorials.ws/electromagnetism/magnetic-hysteresis.html`

[5] Mörée, Gustav and Mats Leijon, 2023, "Review of Hysteresis Models for Magnetic Materials", *Energies*, vol. 16, no. 9, 3908, [Online]. Available : `https://doi.org/10.3390/en16093908`

[6] Gan J. and Zhang X., 2019, "A review of nonlinear hysteresis modeling and control of piezoelectric actuators", *AIP Advances*, vol. 9, 040702, [Online]. Available : `https://www.researchgate.net/publication/332430919_A_review_of_nonlinear_hysteresis_modeling_and_control_of_piezoelectric_actuators/citations`

[7] J.P. Lien, Alexander York, Tiegang Fang, Gregory D. Buckner, 2010, "Modeling piezoelectric actuators with Hysteretic Recurrent Neural Networks", *Sensors and Actuators A: Physical*, vol 163, no. 2, pp 516-525, [Online]. Available : `https://www.sciencedirect.com/science/article/pii/S0924424710003717`

[8] Gu, Guoying, Zhu, Limin and Su, Chun-Yi, 2013, "Modeling and Compensation of Asymmetric Hysteresis Nonlinearity for Piezoceramic Actuators With a Modified Prandtl–Ishlinskii Model", *IEEE Transactions on Industrial Electronics*, vol. 61, pp 1583-1595.

[9] Janaideh, Mohammad and Al Saaideh, Mohammad and Tan, Xiaobo, 2023, "The Prandtl-Ishlinskii Hysteresis Model: Fundamentals of the Model and Its Inverse Compensator", *IEEE Control Systems*, vol. 43, [Online]. Available : `https://www.researchgate.net/publication/369511038_The_Prandtl-Ishlinskii_Hysteresis_Model_Fundamentals_of_the_Model_and_Its_Inverse_Compensator`

[10] Wang, Wen and Wang, Ruijin and Sang, Zhiqian and Lu, Keqing and Fuming, Han and Wang, Jian and Ju, Bingfeng, 2020, "A new hysteresis modeling and feedforward control of piezoelectric actuators based on asymmetric Prandtl-Ishlinskii model", *Sensors and Actuators A Physical*, vol. 316, pp 112431

[11] Micky Rakotondrabe, 2012, "Classical Prandtl-Ishlinskii modeling and inverse multiplicative structure to compensate hysteresis in piezoactuators". *American Control Conference*, pp.1646-1651, hal-00799726f, [Online]. Available : `https://hal.science/hal-00799726/document`

[12] Ahmed, Khubab, Peng Yan, and Su Li, 2021, "Duhem Model-Based Hysteresis Identification in Piezo-Actuated Nano-Stage Using Modified Particle Swarm Optimization", *Micromachines*, vol. 12, no. 3, pp 315, [Online]. Available : `https://doi.org/10.3390/mi12030315`

[13] Geng Wang and Guoqiang Chen, 2017, "Identification of piezoelectric hysteresis by a novel Duhem model based neural network", *Sensors and Actuators A: Physical*, vol. 264, pp 282-288, [Online]. Available : `https://www.sciencedirect.com/science/article/pii/S0924424717311901`

[14] Konstantinos Krikelis and Koos van Berkel and Maarten Schoukens, 2021, "Artificial Neural Network Hysteresis Operators for the Identification of Hammerstein Hysteretic Systems", *IFAC-PapersOnLine*, vol. 54, no. 7, pp 702-707, [Online]. Available : `https://www.sciencedirect.com/science/article/pii/S2405896321012179`

[15] X.H. SHI, Y.C. LIANG, H.P. LEE, W.Z. LIN, X. XU and S.P. LIM., 2004, "IMPROVED ELMAN NETWORKS AND APPLICATIONS FOR CONTROLLING ULTRASONIC MOTORS", *Applied Artificial Intelligence*, vol. 18, no. 7, pp 603-629

[16] Rodríguez-Torres, Andrés and López-Pacheco, Mario and Morales-Valdez, Jesús and Yu, Wen and Díaz, Jorge G., 2022, "Robust Force Estimation for Magnetorheological Damper Based on Complex Value Convolutional Neural Network", *Journal of Computational and Nonlinear Dynamics*, vol. 17, no. 12, pp 121003, [Online]. Available : `https://doi.org/10.1115/1.4055731`

[17] Young-Rae Ko, Yoonkyu Hwang, Minji Chae, Tae-Hyoung Kim, 2017, "Direct identification of generalized Prandtl–Ishlinskii model inversion for asymmetric hysteresis compensation", *ISA Transactions*, vol. 70, pp 209-218, [Online]. Available : `https://www.sciencedirect.com/science/article/pii/S0019057817304871`

[18] Gan, Jinqiang and Zhang, Xianmin and Wu, Heng, 2016, "A generalized Prandtl-Ishlinskii model for characterizing the rate-independent and rate-dependent hysteresis of piezoelectric actuators", *Review of Scientific Instruments*, vol. 87, no. 3, pp 035002, [Online]. Available : `https://doi.org/10.1063/1.4941941`

[19] Mohammad Al Janaideh, Pavel Krejčí, Giselle A. Monteiro, 2024, "emory reduction of rate-dependent Prandtl–Ishlinskii compensators in applications on high-precision motion systems", *Physica B: Condensed Matter*, vol. 677, pp 415595, [Online]. Available : `https://www.sciencedirect.com/science/article/pii/S0921452623009626`

[20] Yang L, Zhong R, Li D, Li Z., 2022, "A fractional-order Duhem model of rate-dependent hysteresis for piezoelectric actuators", *Measurement and Control*, vol. 55, no. (9-10), pp 974-982, [Online]. Available : `https://doi.org/10.1177/00202940221092140`

[21] Gan, Jinqiang, Zhen Mei, Xiaoli Chen, Ye Zhou, and Ming-Feng Ge., 2019, "A Modified Duhem Model for Rate-Dependent Hysteresis Behaviors", *Micromachines*, vol. 10, no. 10, pp 680, [Online]. Available : `https://doi.org/10.3390/mi10100680`

[22] Fuad Mohammad Naser and Fayçal Ikhouane, 2013, "Characterization of the Hysteresis Duhem Model", *IFAC Proceedings Volumes*, vol. 46, no. 12, pp 29-34, [Online]. Available : `https://www.sciencedirect.com/science/article/pii/S1474667015339306`

[23] Klemenc, Jernej and Šeruga, Domen and Nagode, Aleš and Nagode, Marko, 2019, "Comprehensive Modelling of the Hysteresis Loops and Strain–Energy Density for Low-Cycle Fatigue-Life Predictions of the AZ31 Magnesium Alloy", *Materials*, vol. 12, pp 3692, [Online]. Available : `https://www.researchgate.`

net/publication/337124422_Comprehensive_Modelling_of_the_Hysteresis_Loops_and_Strain-Energy_Density_for_Low-Cycle_Fatigue-Life_Predictions_of_the_AZ31_Magnesium_Alloy

[24] Giorgi, Claudio and Morro, Angelo, 2021, "A Thermodynamic Approach to Rate-Type Models of Elastic-Plastic Materials", *Journal of Elasticity*, vol. 147, [Online]. Available : https://www.researchgate.net/publication/337124422_Comprehensive_Modelling_of_the_Hysteresis_Loops_and_Strain-Energy_Density_for_Low-Cycle_Fatigue-Life_Predictions_of_the_AZ31_Magnesium_Alloy

[25] Xu, Bin and Paillard, Charles and Dkhil, Brahim and Bellaiche, L., 2016, "Pinched hysteresis loop in defect-free ferroelectric materials", *Phys. Rev. B*, vol. 94, no. 14, pp 140101, [Online]. Available : https://link.aps.org/doi/10.1103/PhysRevB.94.140101

[26] Jiazeng Shan and Hanqing Zhang and Yuting Ouyang and Weixing Shi, 2020, "Data-driven damage tracking and hysteresis evaluation of earthquake-excited structures with test validation", *Engineering Structures*, vol. 207, pp 110214, [Online]. Available : https://www.sciencedirect.com/science/article/pii/S0141029619331955

[27] Wang, Xiaodong and Ye, Meiying, 2008, "Hysteresis and nonlinearity compensation of relative humidity sensor using support vector machines", *Sensors and Actuators B: Chemical*, vol. 129, pp 274-284, [Online]. Available : https://www.researchgate.net/publication/222000254_Hysteresis_and_nonlinearity_compensation_of_relative_humidity_sensor_using_support_vector_machines/citations

[28] Fouda, Mohammed E. and Majzoub, Sohaib and Radwan, Ahmed, 2020, "Pinched hysteresis loops in non-linear resonators", *IET Circuits, Devices and Systems*, vol. 15

[29] Wikipedia contributors, 2024 April 4, "Feature scaling", *Wikipedia, The Free Encyclopedia*, Version ID: 1217163749, https://en.wikipedia.org/w/index.php?title=Feature_scaling&oldid=1217163749

[30] Wikipedia contributors, 2024 March 9, "Standard score", *Wikipedia, The Free Encyclopedia*, Version ID: 1212815625, https://en.wikipedia.org/w/index.php?title=Standard_score&oldid=1212815625

[31] Wikipedia contributors, 2024 May 5, "Savitzky–Golay filter", *Wikipedia, The Free Encyclopedia*, Version ID: 1226420909, https://en.wikipedia.org/w/index.php?title=Savitzky%E2%80%93Golay_filter&oldid=1226420909

[32] Wikipedia contributors, 2024 May 30, "Wavelet", *Wikipedia, The Free Encyclopedia*, Version ID: 1222290972, https://en.wikipedia.org/w/index.php?title=Wavelet&oldid=1222290972

[33] Henri P. Gavin, 2024, "The Levenberg-Marquardt algorithm for nonlinear least squares curve-fitting problems", *Department of Civil and Environmental Engineering Duke University*, [Online]. Available : https://people.duke.edu/~hpgavin/ExperimentalSystems/lm.pdf

[34] Konstantinos G. Derpanis, 2010, "Overview of the RANSAC Algorithm", [Online]. Available : http://www.cs.yorku.ca/~kosta/CompVis_Notes/ransac.pdf

Apendix

Appendix A : raw data

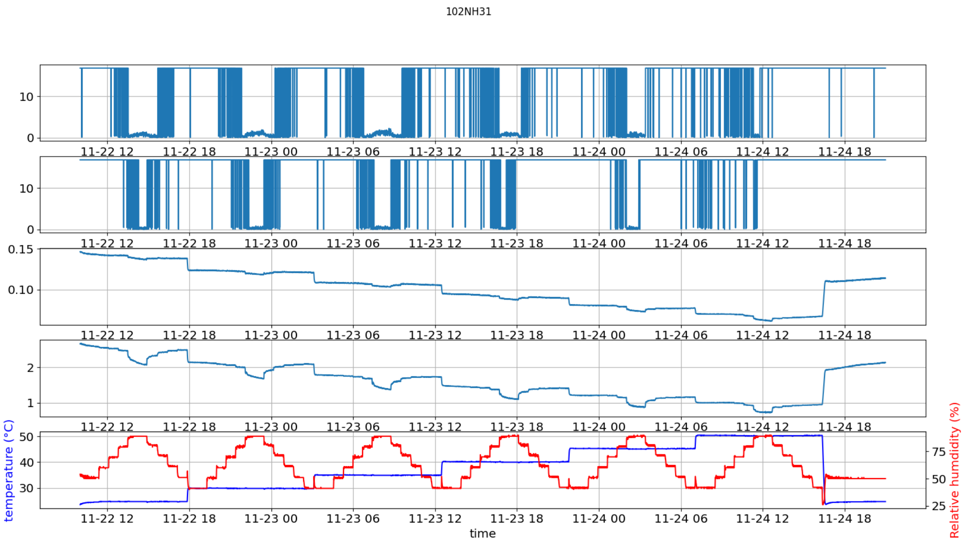

Figure 6.1: 1-4 channel of sensor #102 for the first experiment

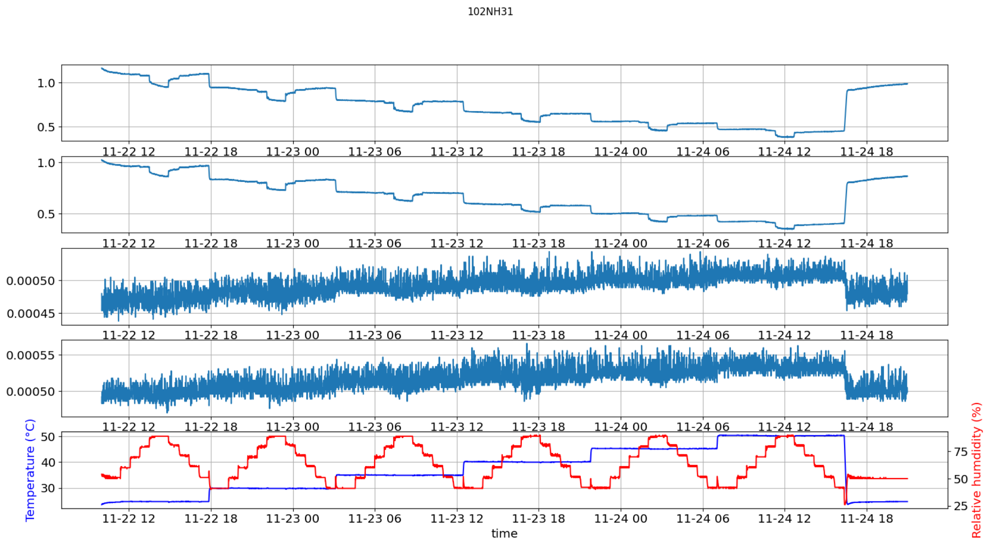

Figure 6.2: 5-8 channel of sensor #102 for the first experiment

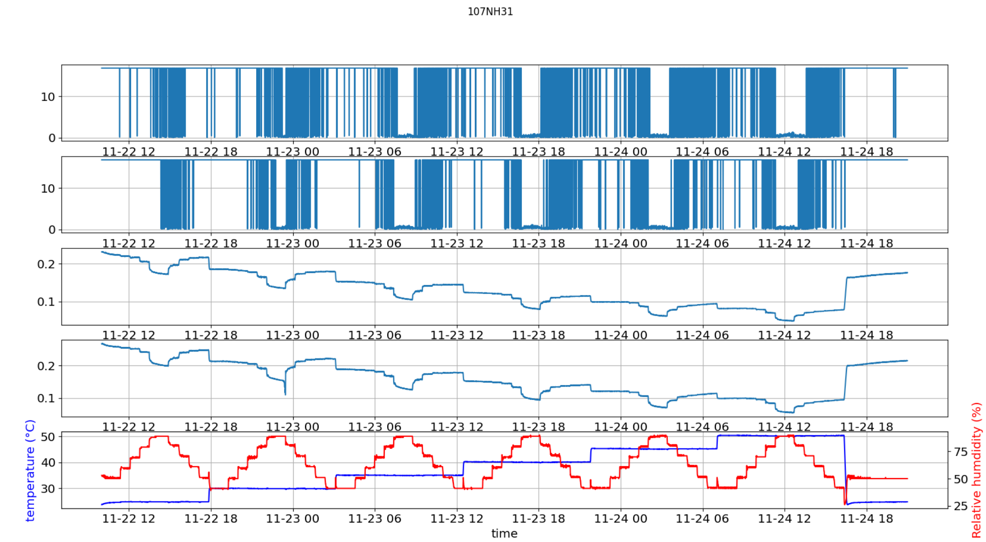

Figure 6.3: 1-4 channel of sensor #107 for the first experiment

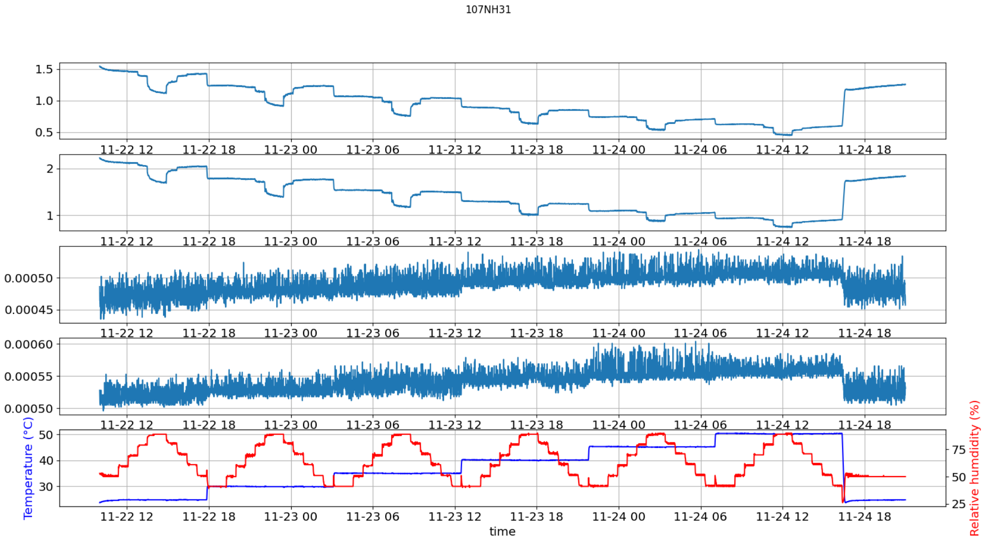

Figure 6.4: 5-8 channel of sensor #107 for the first experiment

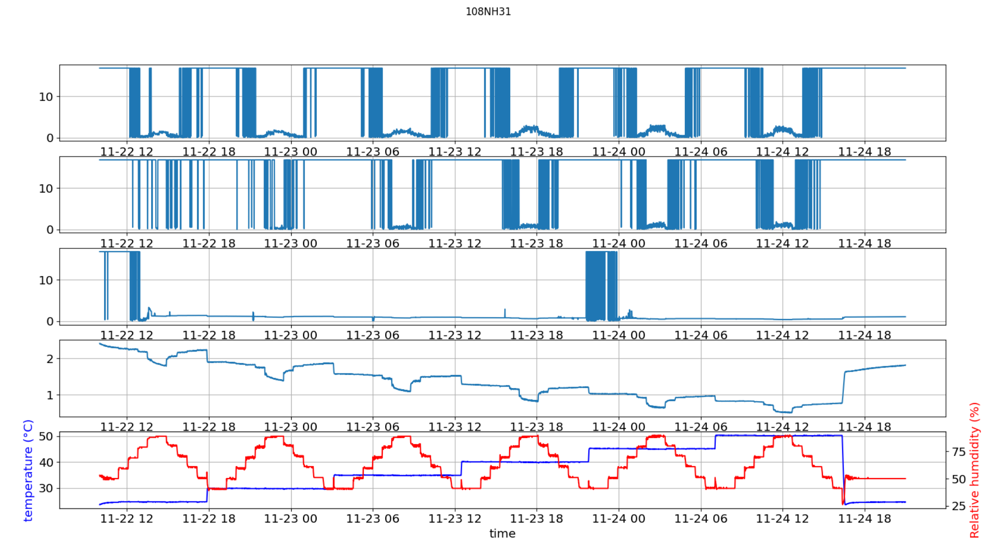

Figure 6.5: 1-4 channel of sensor #108 for the first experiment

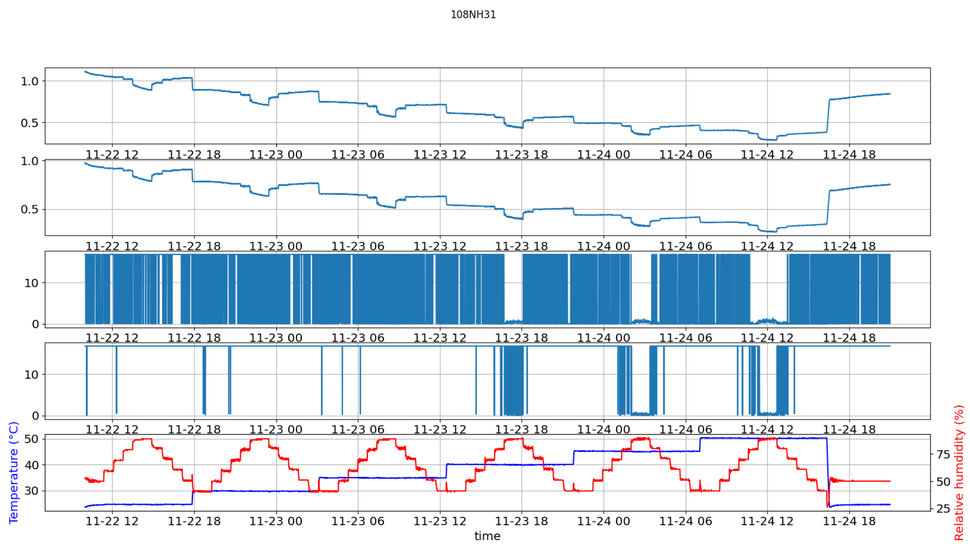

Figure 6.6: 5-8 channel of sensor #108 for the first experiment

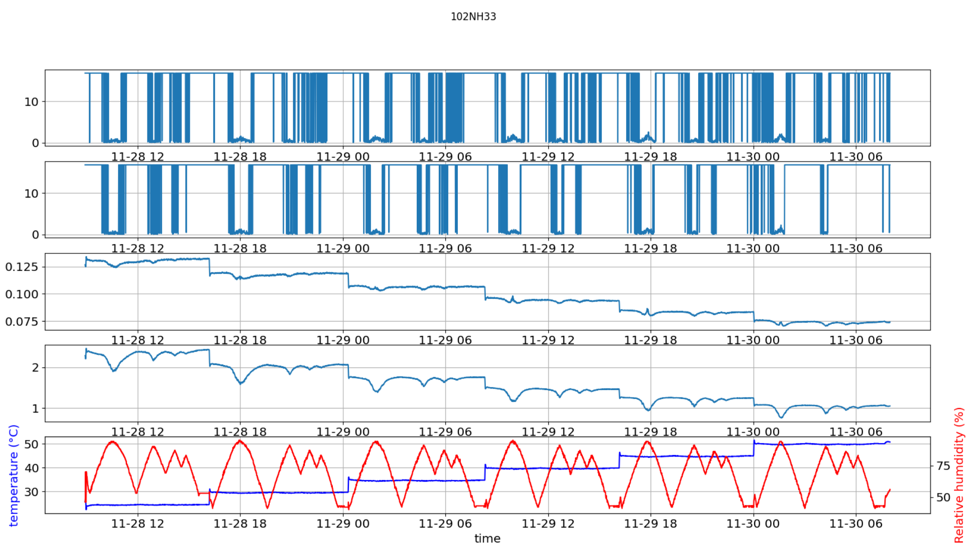

Figure 6.7: 1-4 channel of sensor #102 for the second experiment

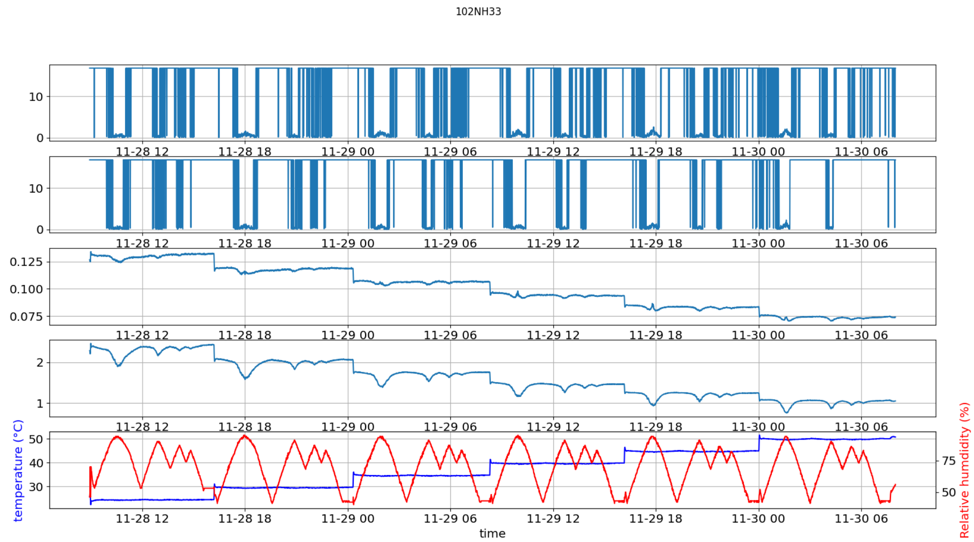

Figure 6.8: 5-8 channel of sensor #102 for the second experiment

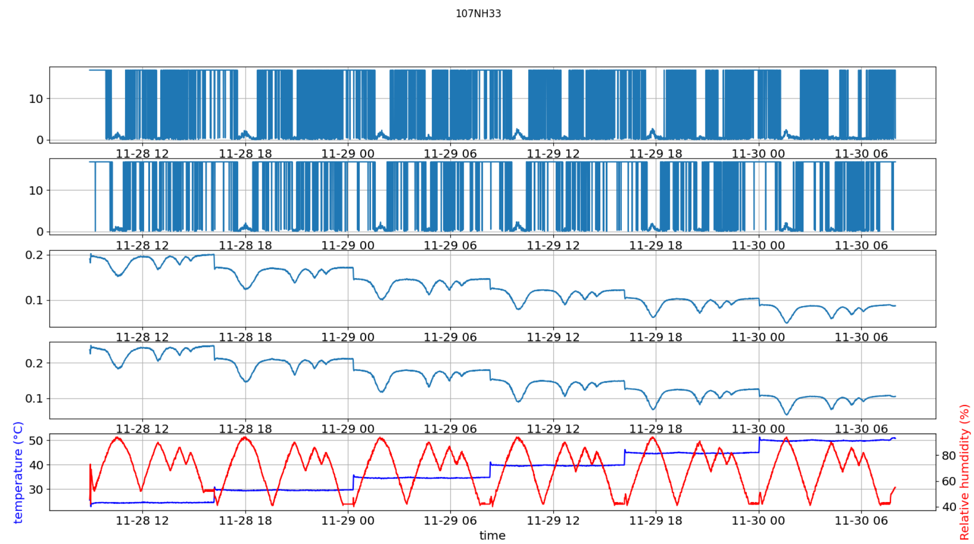

Figure 6.9: 1-4 channel of sensor #107 for the second experiment

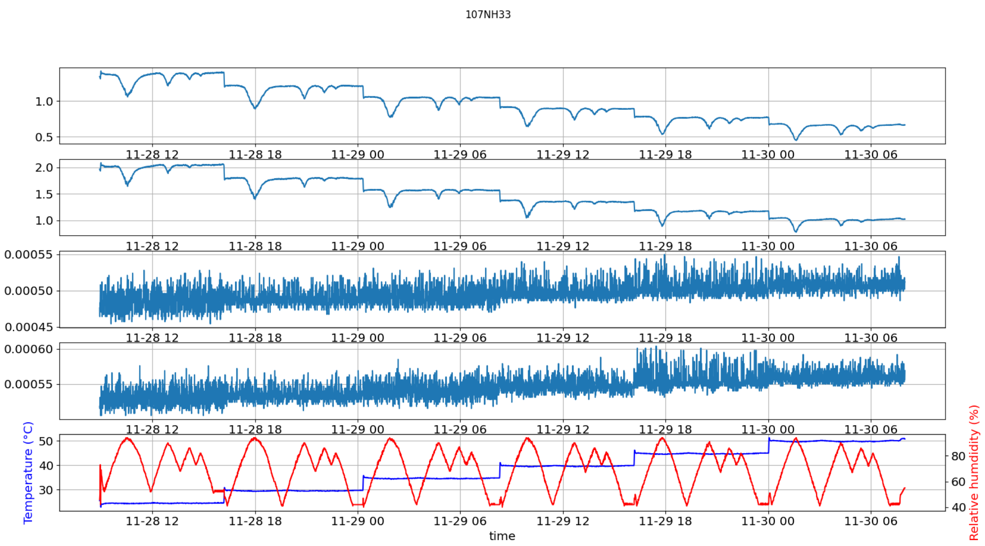

Figure 6.10: 5-8 channel of sensor #107 for the second experiment

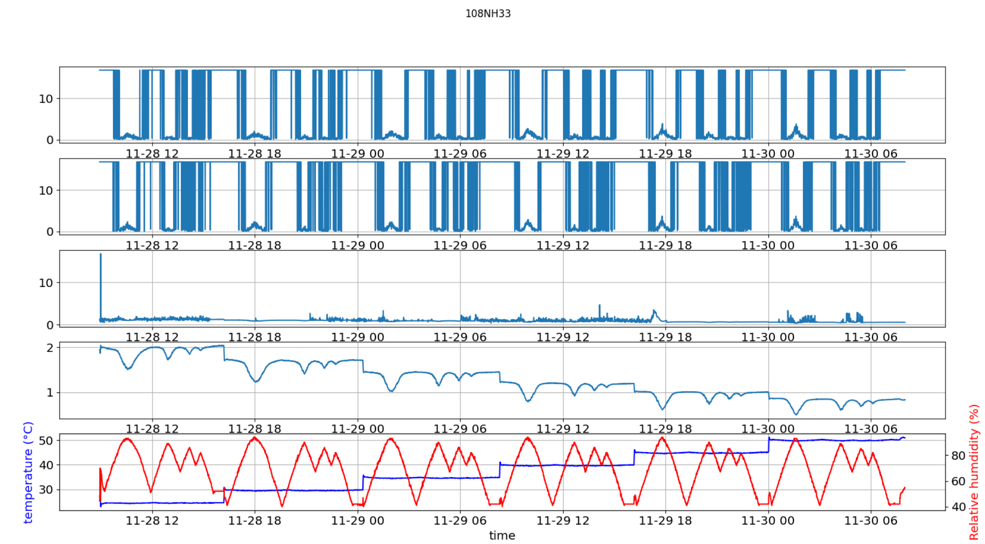

Figure 6.11: 1-4 channel of sensor #108 for the second experiment

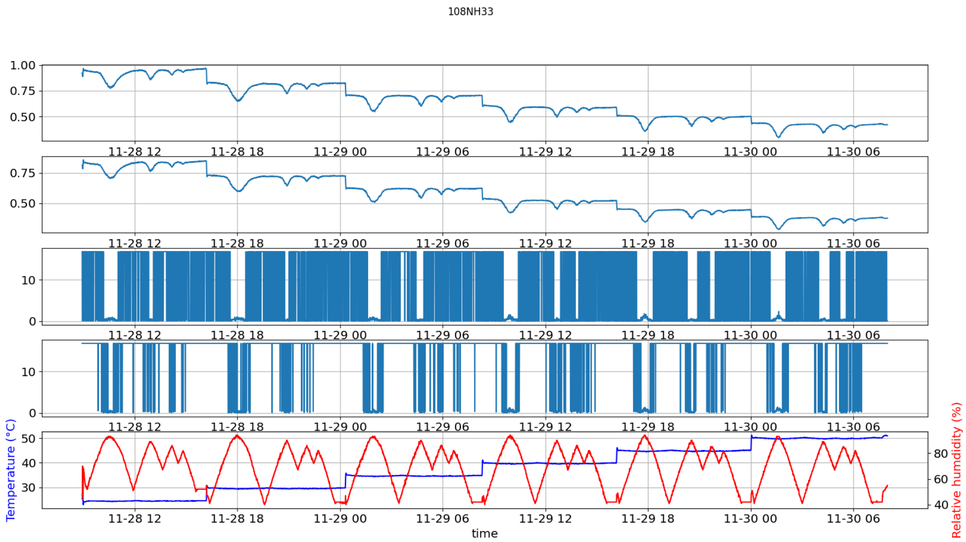

Figure 6.12: 5-8 channel of sensor #108 for the second experiment

Appendix B : Hysteresis curve experience 1

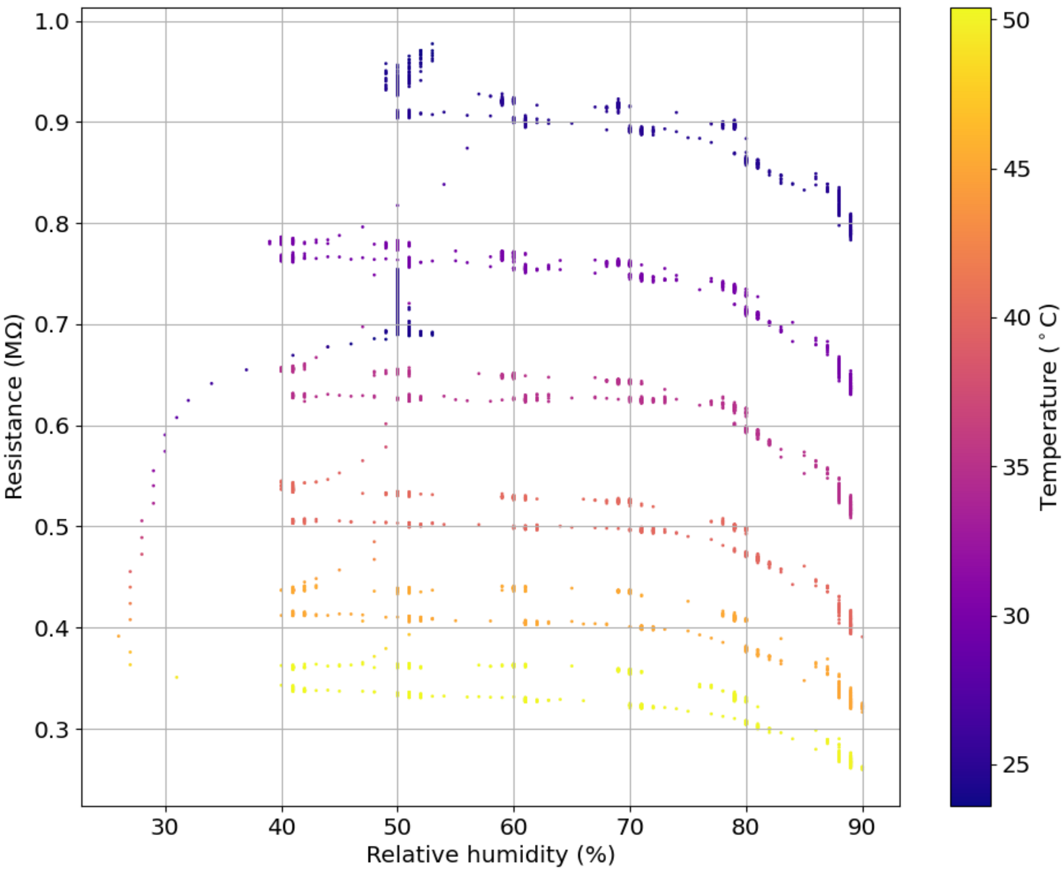

Figure 6.13: Hysteresis curve for the first experience

Appendix C : Threshold

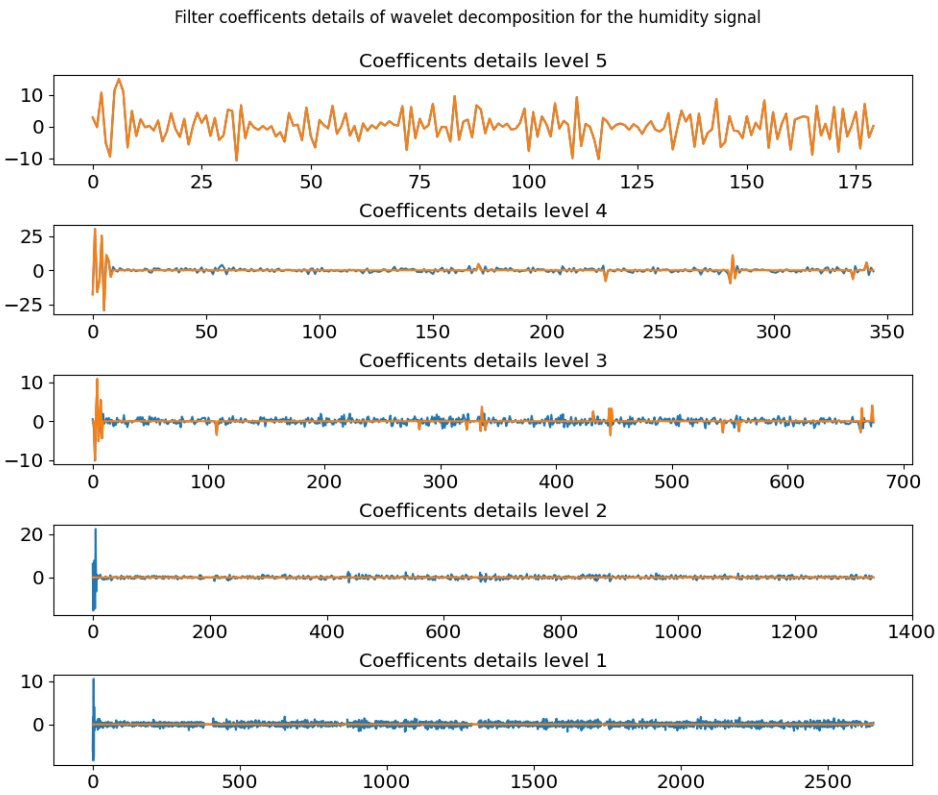

Figure 6.14: Coefficient threshold of the humidity wavelet filter

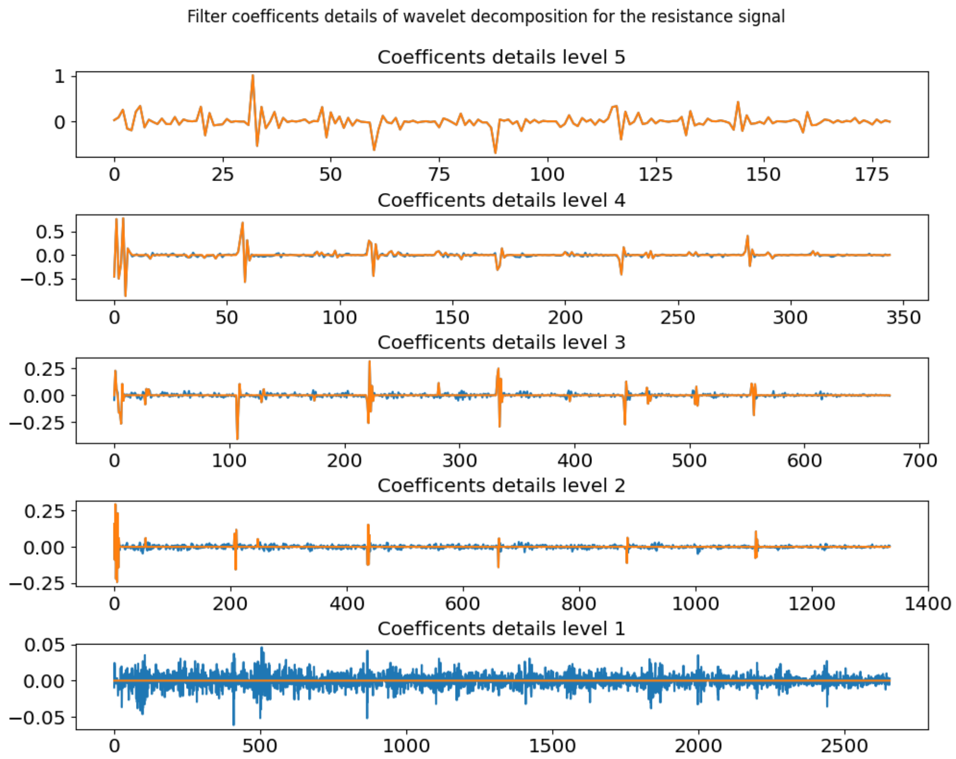

Figure 6.15: Coefficient threshold of the resistance wavelet filter

UNIVERSITÉ CATHOLIQUE DE LOUVAIN
École polytechnique de Louvain
Rue Archimède, 1 bte L6.11.01, 1348 Louvain-la-Neuve, Belgique | **www.uclouvain.be/epl**